ISSN 0234-5366

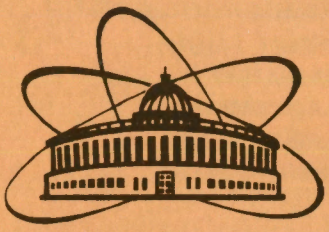

ОБЪЕДИНЕННЫЙ
ИНСТИТУТ
ЯДЕРНЫХ
ИССЛЕДОВАНИЙ

JOINT INSTITUTE
FOR NUCLEAR
RESEARCH

4[61]-93

КРАТКИЕ СООБЩЕНИЯ ОИЯИ

JINR RAPID COMMUNICATIONS

ДУБНА

Объединенный институт ядерных исследований
Joint Institute for Nuclear Research

4[61]-93

КРАТКИЕ СООБЩЕНИЯ ОИЯИ
JINR RAPID COMMUNICATIONS

сборник
collection

Дубна 1993

ОГЛАВЛЕНИЕ
CONTENTS

УДК 539.17:621.384.63

USING OF INTERNAL TARGETS IN THE NUCLOTRON

A.S.Artiomov

The potentialities of investigation of nucleus-nucleus collisions on internal beams of the Nuclotron (a specialized superconducting strong-focusing accelerator of nuclei at the LHE) are discussed. Emphasis is made on the importance of the change of beam parameters as a result of ion-internal target interaction. Analytical expressions for the evolution of beam parameters are obtained. The target station, which was used in a first experiment at the Nuclotron, is described. The time change of the ion flux interacting with an internal target, which was controlled by means of target radiation, agrees with theoretical estimations.

The investigation has been performed at the Laboratory of High Energies, JINR.

Использование внутренних мишеней в Нуклотроне

А.С.Артемов

Обсуждаются потенциальные возможности исследования ядро-ядерных столкновений на внутренних пучках в Нуклотроне (специализированного сверхпроводящего жесткофокусирующего ускорителя ядер в ЛВЭ). Подчеркивается важность учета изменения параметров пучка в результате взаимодействия ионов с внутренней мишенью. Получены аналитические выражения эволюции параметров пучка во времени. Описана станция внутренних мишеней, которая была использована в первом эксперименте на Нуклотроне. Изменение во времени потока ионов, взаимодействующего с внутренней мишенью, контролировалось по излучению мишени и согласуется с теоретическими оценками.

Работа выполнена в Лаборатории высоких энергий ОИЯИ.

1. Introduction

At present we have a clear notion of the general picture of nucleus-nucleus collisions over a wide energy range that makes it possible to plan confidently the development of accelerator facilities and to form installations on nuclear beams. Relativistic nuclear physics deals with the study of processes in which the constituents of nuclear matter move with relative velocities close to the velocity of light. The asymptotic character of such natural phenomena has played a decisive role in a detailed construction plan and cost estimate of the Nuclotron, a specialized superconducting accelerator of relativistic nuclei at the LHE of the Joint Institute for Nuclear

Research in Dubna [1]. This accelerator provides new possibilities for internal target technique. Taking into account a small vacuum chamber of the strong focusing machine, one can place detectors closer to the target and construct a setup with a solid angle approaching to 4π. Choosing the internal target thickness, one can detect various products of the fragmentation of colliding nuclei and obtain information on them without deterioration of average beam luminosity (see below). This feature is important to record complete information on nucleus-nucleus collision.

2. Internal target effects

As a result of nucleus-internal target interaction, new particles are created and beam parameters are evaluated. Using the Courant-Snyder formalism [2] for transverse phase ellipses and taking initially the Gaussian distribution of (Y_i, Y_i')-coordinates over ions in a beam, the following correlation can be obtained

$$\langle(\hat{Y}_i)^2\rangle = 2\beta_i\varepsilon_i^{(0)}(\eta)/\eta^2. \tag{1}$$

Here $\langle\ \rangle$ is the mean value over all the ions in a beam, $Y_i = X, Z$ are the horizontal (radial) and vertical (axial) displacements from the equilibrium orbit, respectively; $(\hat{Y}_i)^2 = Y_i^2 + (\alpha_i Y_i + \beta_i Y_i')^2$; $\pi\varepsilon_i^{(0)}(\eta)$ are the emittance areas before ion-internal target interaction corresponding to η standard deviations in the distributions and enclosing a ξ part of all ions in the beam ($\eta = 1 \to \xi = 0.384$, $\eta = 2 \to \xi = 0.865$, $\eta = 3 \to \xi = 0.989$); β_i, α_i, D_i, D_i', $\gamma_i = (1 + \alpha_i^2)/\beta_i$ (see below) are the parameters of the accelerator at the target location. When a fast ion is nondestructible after the j-traversal of the internal target, the change $\delta Y_{i,j}'$ of the trajectory slope and the relative momentum deviation $\delta_j = \Delta p_j / p$ take place. The deviation $\delta Y_{i,j}$ behind the target can be usually neglected. Assuming the number of betatron oscillations per turn $Q_i = m_i / n_i$ (m_i and n_i are the whole numbers), $\mu_i = 2\pi Q_i$ and using Twiss's transport matrices (see, for example, [3]), we obtained the deviations

$$\delta Y_i(n_i) = \beta_i \sum_{j=1}^{n_i} (\sin j\mu_i)\,\delta Y_{i,j}' + D_i \sum_{j=0}^{n_i-1} [\cos j\mu_i + \alpha_i \cdot \sin j\mu_i]\,\delta_{j+1} +$$

$$+ D_i' \beta_i \sum_{j=1}^{n_i-1} (\sin j\mu_i)\,\delta_j, \tag{2}$$

$$\delta Y_i'(n_i) = \sum_{j=1}^{n_i} (\cos j\mu_i - \alpha_i \cdot \sin j\mu_i) \cdot \delta Y_{i,j}' +$$

$$+ \sum_{j=0}^{n_i-1} [D_i'(\cos j\mu_i - \alpha_i \cdot \sin j\mu_i) - \gamma_i D_i \sin j\mu_i]\, \delta_{j+1}, \qquad (3)$$

after an «elementary act» of ion-internal target interaction in the absence of oscillation damping (effect n_i of target traversals and following turns). Here and below we suppose that ions traverse a homogeneous target every turn and residual gas effects are negligible. When the mean energy loss per target traversal is compensated by an appropriate synchrotron acceleration in the rf-cavity (recirculation mode of accelerator operation), the $\delta Y_i(n_i)$ and $\delta Y_i'(n_i)$ distributions with the mean values of $\overline{\delta Y_i(n_i)} = \overline{\delta Y_i'(n_i)} = 0$ and their mean square deviations are independent of the «elementary act» number. Thus, from the fundamental limit theorem of probability theory, we can assume that the resulting (Y_i, Y_i')-distributions after many «elementary acts» of ion-internal target interaction will be also Gaussian. From this and using correlation (1), the following expression on the evolution of transverse emittances $\varepsilon_i^{(N)}(\eta)$ can be obtained

$$\varepsilon_i^{(N)}(\eta) = \varepsilon_i^{(0)} + 0.5N\beta_i \eta^2 \overline{(\delta Y')^2} +$$

$$+ 0.5N\eta^2 [\gamma_i D_i^2 + 2\alpha_i D_i D_i' + \beta_i (D_i')^2] \overline{\delta^2}, \qquad (4)$$

where N is the Number of target traversals, $\overline{(\delta Y')^2}$ and $\overline{\delta^2}$ are the mean square deviations in angle and relative momentum after the target traversal.

For small synchrotron oscillation amplitudes with Gaussian distribution in longitudinal $(\Delta\varphi, \delta)$-phase space ($\Delta\varphi$ is the rf-phase lag with respect to the φ_s-phase of the synchronous particle) and from formal analogy between upright longitudinal and similar transverse ($\alpha_l = 0$) phase ellipses, one can obtain the following equation for the evolution of longitudinal emittance

$$\varepsilon_l^{(N)}(\eta) = \varepsilon_l^{(0)} + 0.5N\beta_l \cdot \eta^2 \cdot \overline{\delta^2}. \qquad (5)$$

Here $\varepsilon_l^{(0)}$ is the initial longitudinal emittance, $\beta_l = h\sqrt{(|\zeta| 2\pi\, p\beta c)/(ZU\cos\varphi_s)}$, $h = \omega_{rf}/\omega_s$ is the hadronic number of rf-cavity; ω_s is the frequency of the synchronous particle turn, $\zeta = \delta \cdot (\Delta\omega/\omega)$ is the longitudinal dispersion of the accelerator, U is the volt-

age amplitude of rf-cavity, p, βc, Z and are the momentum, velocity and charge number of the ions, respectively. For $\eta = 1$ and $\alpha_i = 0$ eqs.(4,5) coincide with the result of ref. [4].

For high energy ions Coulomb scattering, elastic (diffraction) and inelastic nuclear scattering in the target take place (see, for example, [5]). Therefore the resulting $\delta Y'_{i,j}$ and δ_j distributions have a complex form and depend strongly on the target thickness. The total cross sections of above-mentioned interactions can be estimated by $\sigma_c \approx 10^{-20}\,(Z/\beta)^2 Z_0^{4/3}$ [cm^2], $\sigma_d \approx \sigma_{in}$ and $\sigma_{in} \approx 6\cdot 10^{-26}\,(A^{1/3} + A_0^{1/3})$ [cm^2], respectively. Here A is the mass number of the ions, Z_0 and A_0 are the charge and mass numbers of the target. Because of the large Coulomb differential cross section for small angles its scattering defines evolution of transverse and longitudinal beam emittances. For thin targets the values $\overline{(\delta Y')^2}$ and $\overline{\delta^2}$ in eqs.(4,5) can be obtained taking into account only single Rutherford scattering from a screened potential and the results of ref. [6]

$$\overline{(\delta Y')^2} \approx 5\cdot 10^{-8}\cdot t\cdot A_0^{-3}(ZZ_0/\gamma\beta^2)^2\,[\ln(\theta_{cm}/\sqrt{2}\,\theta_{min}) - 0.25], \quad (6)$$

$$\overline{\delta^2} \approx 2\cdot 10^{-5}\cdot t\cdot \frac{Z^2 Z_0^{5/3}}{\beta^3 A A_0^2}. \quad (7)$$

Here $\gamma = (1-\beta^2)^{-0.5}$, t is the target thickness [g/cm^2], $\theta_{min} \approx$ $\approx 2.8\cdot 10^{-6} Z_0^{1/3}/(\beta\gamma A_0)$ is the atomic screening angle of the target, $\theta_{cm} \approx 2.3\cdot 10^{-3} ZZ_0/\,[\beta^2\gamma A(A^{1/3} + A_0^{1/3})]$ is the maximum angle of the Rutherford scattering determined by nuclear radii of an ion and a target. The growth of beam emittances, inelastic nuclear scattering and large angle elastic scattering in a single ion passage through the target lead to the beam losses. If we take into account only first channel the following expression of the time evolution of the circulating beam intensity (in relative units) can be obtained

$$I_1(\tau) = \prod_i I_{1i} = \prod_i [erf(\eta/\sqrt{\xi_i})/erf(\eta)]^2, \quad (8)$$

where $\xi_i = \varepsilon_i^{(N)}(\eta)/A_i \geq 1$, $I_{1i}(\tau) = 1$ otherwise, $\tau = NP/\beta c$, A_i is the ring acceptance in X or Z directions, $erf(x)$ is the error function and P is the ring

circumference. This result agrees with the more complex expressions in refs. [3,4], where the Fokker — Planck method is used. Taking into account only angular scattering, the total cross section, which leads to the loss of the ion in a single passage through the target, is obtained as

$$\sigma_t = 0.5\sigma_c(\theta_{xa}^{-2} + \theta_{za}^{-2} - 2\theta_{cm}^{-2}) +$$

$$+ 0.5\sigma_{in}\,[4 - erf\,(\theta_{xa} / 2\theta_d) - erf\,(\theta_{za} / 2\theta_d)]. \qquad (9)$$

Here $\theta_{ia}^2 \approx A_i / \pi \beta_i$ $(i = x,z)$, $\theta_d \approx 0.15[A(\gamma^2 - 1)^{0.5}(A^{1/3} + A_0^{1/3})]^{-1}$, and Gaussian approximation of the central maximum of the plane diffractional nuclear scattering is used. In eq. (9) we must assume $\theta_{ia} = \theta_{cm}$ when $\theta_{ia} > \theta_{cm}$. Depending on the collision energy and the type of colliding nuclei, in eq. (9) the different terms dominate. The combination of eqs. (8,9) yields to the following expression of the time evolution of the circulating beam intensity

$$I(\tau) = I_1(\tau) \cdot \exp(-\tau/T), \qquad (10)$$

where $T = PA_0/(6 \cdot 10^{23} t \beta c \sigma_t)$. For estimation of the beam lifetime (T_b) the expression $I_1(\tau)$ can be approximated by $\exp(-\tau/T_{ef})$ starting from the minimum time τ_i corresponding to $\xi_i = 1$. Thus one can assume

$$T_b \approx \begin{cases} T/(1 + T/T_{ef}) & \text{if min } \tau_i < T; \\ T & \text{otherwise;} \end{cases} \qquad (11)$$

where $T/T_{ef} = \sigma_{ef}/\sigma_t$, σ_{ef} is the effective cross section of the ion loss depending on the beam emittances and the accelerator parameters (see eqs. (4—8)). The luminosity is the product of a beam current and a target thickness averaged over time. Taking into account eq. (11), the luminosity L_c averaged over the cycle time T_c of the accelerator ($T_c > T_b$) is equal to

$$L_c = N_0/[T_c(\sigma_t + \sigma_{ef})], \qquad (12)$$

and independent of the target thickness. Here N_0 is the number of the storage ions before ion-internal target interaction, $\sigma_{ef} = 0$ or $\neq 0$ according to the condition in eq. (11). The equivalent target thickness for an external beam is defined as

$$t_{eq}\,[\text{g/cm}^2] = \frac{A_0}{6 \cdot 10^{23}(\sigma_t + \sigma_{ef})}. \qquad (13)$$

3. Target station arrangement

The linear area of the Nuclotron with an internal target station is the installation with its own independent vacuum pumps. It can operate both as a part of the beam transport line of the Nuclotron and independently of it when the accelerator is off. The independent vacuum pumping and dismountable design of the station allow one to change functional possibilities of this installation operatively and without an influence on the vacuum and cryogenic systems of the other Nuclotron areas. We can realize the mounting of the next batch of internal targets or elements for following irradiation on the internal beam of the Nuclotron and also the total replacement of the station for another experiment. Thus, at this installation one can use various types of internal targets (foils, thread-like, jets, beams, etc.), test new methods of beam diagnostics and realize certain experiments analogous to those with a solid angle approaching to 4π on an external beam. Taking into account the supposed beam intensities in a first stage of operation (see [1]), emittances and parameters of the Nuclotron (see [7]), one can expect the following mean luminosities [$cm^{-2}s^{-1}$]:

$$L_c(d \to 1\ A\cdot GeV) \approx 4\cdot 10^{33}(C, CH_2),\ 7\cdot 10^{32}(Cu),\ 10^{32}(Au);$$

$$L_c(d \to 6\ A\cdot GeV) \approx 4\cdot 10^{33}(C, CH_2),\ 2\cdot 10^{33}(Cu),\ 10^{33}(Au);$$

$$L_c(^{12}C \to 1\ A\cdot GeV) \approx 4\cdot 10^{32}(C, CH_2),\ 10^{32}(Cu),\ 2\cdot 10^{31}(Au);$$

$$L_c(^{12}C \to 6\ A\cdot GeV) \approx 6\cdot 10^{32}(C, CH_2),\ 3\cdot 10^{32}(Cu),\ 2\cdot 10^{32}(Au);$$

$$L_c(^{40}Ar \to 1\ A\cdot GeV) \approx 2\cdot 10^{30}(C, CH_2),\ 6\cdot 10^{29}(Cu),\ 10^{29}(Au);$$

$$L_c(^{40}C \to 6\ A\cdot GeV) \approx 2\cdot 10^{30}(C, CH_2),\ 10^{30}(Cu),\ 6\cdot 10^{29}(Au).$$

At the first run we used the target station made of two crossing cylinders of the beam transport line and a larger diameter cylinder with three internal targets. The dimensions and wall thickness (0.5 mm) of the station are optimized to detect second particles by external detectors with a maximum solid angle and minimum losses. The foil targets of CH_2 (1.6 μm thickness), Cu (0.55 μm) and Au (1.7 μm) are hanged up by 9 μm diameter quartz fibres in the *C*-shaped frames mounted vertically on the table rotating by means of a step motor with a high precision. Extraction of all frames with the targets from the beam transport line, choice of a necessary target for experiment and control of its spatial position relative to the transport line axis are realized by means of an electro-optical device constrained with the rotation

axis of the table and the distant control system of the step motor. It allows the target to be introduced into the beam on a controllable depth and time exposition distantly and at a determined time moment relative to the beginning of an ion acceleration cycle. The upper dismountable flange of the station is used to change the frames with the targets. It has a window for visual control on the targets in adjusting and two branch pipes for placing detectors in vacuum.

In a first experiment at the Nuclotron with a deuteron beam several $\Delta E - E$ scintillation telescopes are used to detect secondary protons and deuterons. To control the intensity and lifetime of a part of the deuteron beam interacting with the target, the radiation of the target material is used. The radiation is detected through the window by a photomultiplier tube and by a tandem-microchannel-plate detector in vacuum. The obtained oscillograms indicate the time structure of the coasting beam, and a decrease of intensity in time agrees with theoretical estimations for the used targets and deuteron energy (200 MeV). While adjusting the acceleration mode at the Nuclotron (the absence of targets in the beam transport line), radiation signals corresponding to the bombardment of the station wall by a part of the deuteron beam were episodically observed.

References

1. Baldin A.M. — JINR Commun. E1-92-487, Dubna, 1992.
2. Courant E.D., Snyder H.S. — Ann. Phis. (NY), 1958, 3, p.1.
3. Henri Bruck .— Accelerateurs circulaires de particles, Presses Universitaires de France, Paris 1966.
4. Hinterberger F., Prasuhn D. — Nucl. Instr. and Meth., 1989, A279, p.413.
5. Barashenkov V.S., Toneev V.D. — Interaction of High Energy Particles and Atomic Nuclei with Nuclei (in Russian), Atomizdat, Moscow, 1972.
6. Rossi B. — High Energy Particles, Prentice-Hall, Inc., Englewood Cliffs, NJ, 1952.
7. Vasilishin B.V. et al. — JINR Commun. 9-86-512, Dubna, 1986, in Russian.

Received on September 2, 1993.

УДК 539.172.13.+621.384.668.82

THE FIRST EXPERIMENTS ON NUCLEAR REACTION STUDIES AT NUCLOTRON

A.M.Baldin, S.V.Afanasiev, Yu.S.Anisimov, V.V.Arkhipov, A.S.Artyomov, V.K.Bondarev, O.V.Egorov, A.F.Elishev, V.I.Ilyushchenko, A.Yu.Isupov, V.A.Kashirin, A.N.Khrenov, V.I.Kolesnikov, A.D.Kovalenko, V.A.Kuznetsov, A.G.Litvinenko, A.I.Malakhov, P.K.Maniakov, E.A.Matyushevsky, G.L.Melkumov, I.I.Migulina, T.M.Mironova, A.S.Nikiforov, V.A.Nikitin, P.V.Nomokonov, V.G.Perevozchikov, V.I.Prokhorov, S.G.Reznikov, A.Yu.Semenov, A.B.Shabunov, V.A.Smirnov, P.I.Zarubin, I.Atanasov*, I.Ivanov*, V.N.Penev*

The first run at the new superconducting accelerator Nuclotron has been carried out in July 1993. The experiment was prepared by SPHERE and SYaO collaborations. The beam of deuterons was accelerated up to 200 MeV per nucleon. The spectra of secondary particles were measured using TOF and $\Delta E-E$ techniques. The results of this run indicate good perspectives to carry out experiments at internal target.

The investigation has been performed in the Laboratory of High Energies, JINR.

Первые эксперименты по изучению ядерных реакций на Нуклотроне

А.М.Балдин и др.

В июле 1993 года проведен первый сеанс на новом сверхпроводящем ускорителе Нуклотрон. Эксперимент подготовлен и проведен коллаборациями СФЕРА и СЯО. Пучок дейтронов был ускорен до 200 МэВ/нуклон. С помощью времяпролетной и $\Delta E-E$ методик были измерены спектры вторичных частиц. Результаты сеанса показали наличие хороших перспектив для проведения экспериментов на внутренней мишени.

Работа выполнена в Лаборатории высоких энергий ОИЯИ.

In July 1993 the LHE performed the first experimental run at the new superconducting accelerator Nuclotron. The programme of the experiments at this machine covers a wide range of problems in relativistic nuclear physics (see ref. [1]). The main goal of experimental efforts is the study of the quark-gluon degrees of freedom in nuclei.

*Institute for Nuclear Research and Nuclear Energy, Sofia, Bulgaria

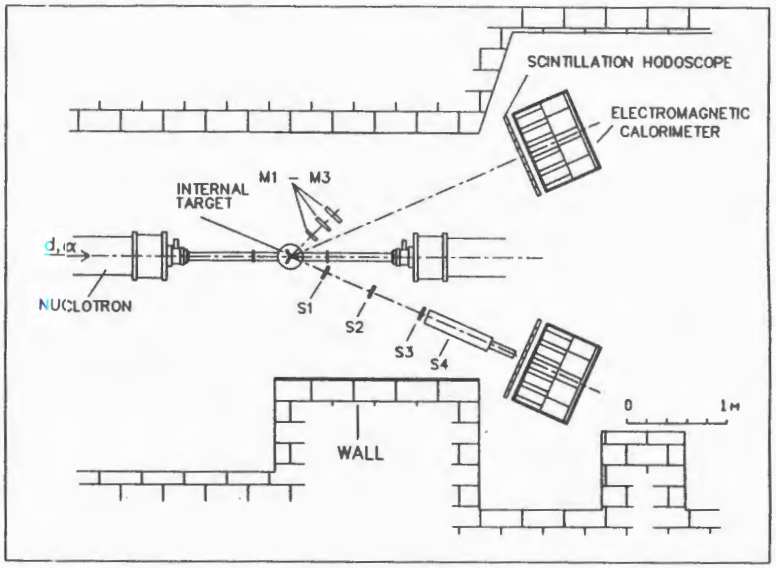

Fig.1. A schematic view of the experimental setup

In this note we report the results of the first experiment with internal target at the Dubna Nuclotron.

The experiment was prepared in the framework of SPHERE and SYaO collaborations. We measured products of interaction of a deuteron beam at the internal target. A schematic view of the setup is shown in fig.1.

The experimental arrangement includes:

— An internal target station. The station operates with polyethylene, copper and gold foils with thickness 1.57, 0.55 and 1.72 μm respectively. Relative target-beam position is controlled by means of a step motor with high precision [2].

— A beam monitoring telescope M1-M3. The telescope consists of three scintillation counters, with dimensions 3x3x0.5 cm^3, 4x4x0.5 cm^3 and 7x7x0.5 cm^3.

— Two 1x1 m^2 scintillation hodoscopes.

— 36-channel lead glass Cherenkov EM calorimeter.

— A detecting telescope. It is composed of four scintillation counters S1—S4 with dimensions of 2x2x0.5 cm^3, 3x3x0.5 cm^3, 4x4x0.5 cm^3 and 7.5x7.5x65 cm^3, respectively. The telescope axis is rotated with respect to the beam direction by 29±1°. The distance between S2 and S3 is 0.5 m, the angular acceptance is about 10^{-3} sr.

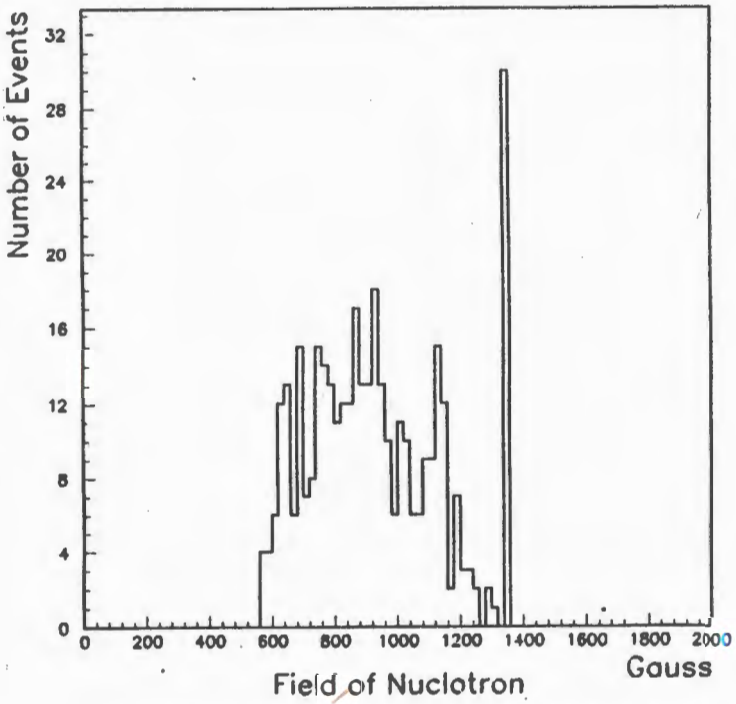

Fig.2. An example of a beam spill of NUCLOTRON at internal target

The power supply of detectors was provided by means of the special high voltage power subsystem [3].

4200 triggers were recorded on polyethylene and empty targets. The statistics of events on copper and gold targets is very small due to a dramatic decrease in the primary beam lifetime for targets with large atomic weight, A. The measurements were taken on increasing the magnetic field of the accelerator at the maximum beam energy 100 and 200 MeV per nucleon. The intensity of the primary beam was $(2+3)\cdot 10^9$ deuterons per spill. An example of a beam spill is shown in fig.2. The rate of beam interactions as a function of magnetic field of the accelerator is presented here.

Secondary particle identification is performed using the TOF information between S2—S3, ΔE-energy loss in S2 and total energy loss in S4. Fig.3 presents the measured $\Delta E-E$ spectrum of secondary particles emitted in the collisions of deuteron beam with polyethylene target. Each event contains two kinematic characteristics for a secondary particle — velocity and kinetic energy, therefore we can reconstruct the mass containment of secondaries. The mass distribution for the first run with the

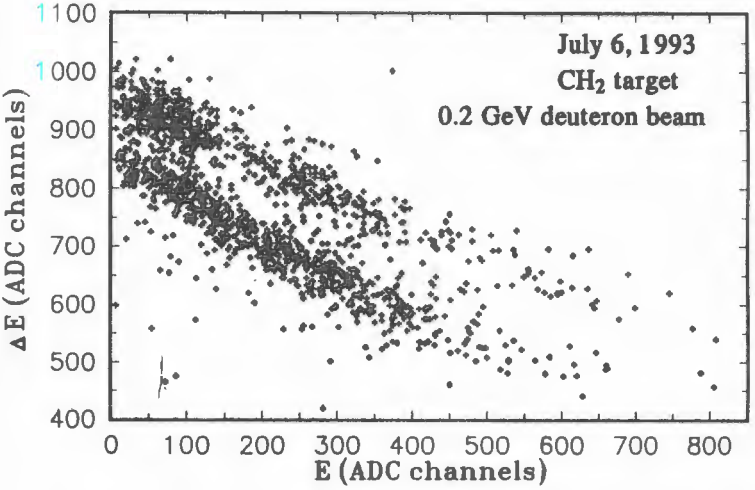

Fig.3. $\Delta E-E$-spectrum of secondary particles on internal target of the Nuclotron

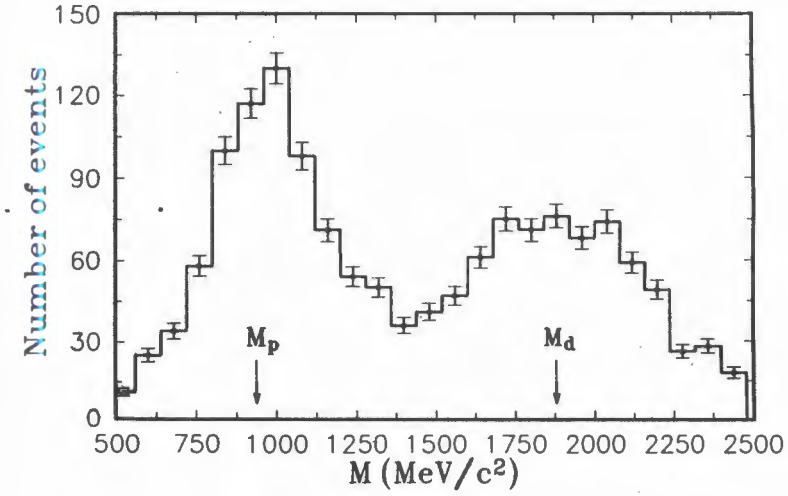

Fig.4. Mass distribution of secondaries

beam energy 100 MeV per nucleon is presented in fig.4. Secondary protons and scattered deuterons are identified in a quite reliable way. Fig.5 shows the experimental spectra for protons and deuterons. The detection thresholds were approximately 25 MeV for protons and 38 MeV for deuterons.

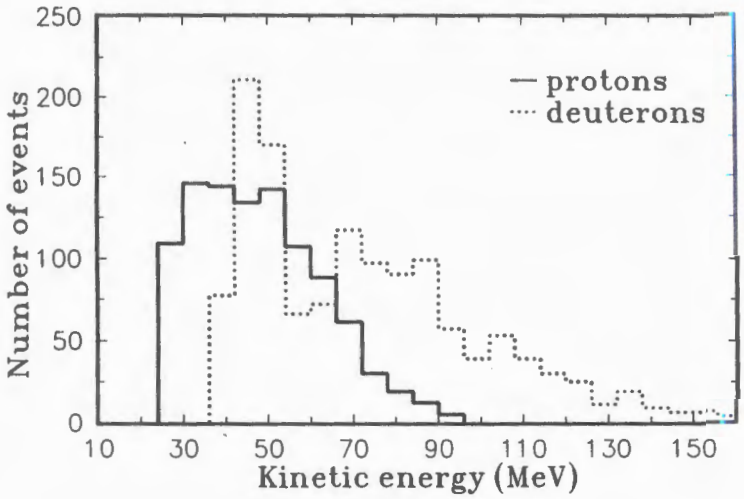

Fig.5. Energy spectra of secondaries

We conclude that homogeneous interactions of an internal beam with a thin target are available now at Nuclotron. This indicates also at the possibility of carrying out future experiments at internal targets simultaneously with the active beam extraction facility.

References

1. Baldin A.M., Malakhov A.I. — JINR Rapid Communications, No.3[60]-93, Dubna, 1993, p.52.
2. Artyomov A.S. — See this volume.
3. Anisimov Yu.S. et al. — JINR Rapid Communications, No.3[60]-93, Dubna, 1993, p.63.

Received on September 28, 1993.

УДК 538.911

FREE FERMION SOLUTION FOR DIMER PROBLEM

R.Hayn*, V.N.Plechko

The new noncombinatorial approach to the dimer problem based on integration over fermionic fields is presented. The partition function of the closed-packed dimer model on the inhomogeneous rectangular lattice is obtained in the form of the Gaussian integral over Grassmann variables.

The investigation has been performed at the Laboratory of Theoretical Physics, JINR and Max Planck Institut für Festkörperforschung, Stuttgart, Germany.

Решение задачи димеров и свободные фермионы

Р.Хайн, В.Н.Плечко

Предложен новый некомбинаторный подход к задаче димеров, основанный на интегрировании по фермионным полям. Для статистической суммы плотноупакованной димерной модели на неоднородной прямоугольной решетке найдено выражение в виде гауссовского интеграла по грассмановым переменным.

Работа выполнена в Лаборатории теоретической физики ОИЯИ и в Институте твердого тела Общества Макса.Планка, Штутгарт, Германия.

1. Introduction

The closed-packed dimer model on the homogeneous rectangular lattice was first solved by Kasteleyn [1] and Temperley and Fisher [2]. Besides its importance for the understanding of the dimer combinatorics itself, this remarkable solution has contributed much to the theory of the 2D Ising model and the other lattice problems in statistical mechanics [3—5]. The dimer models have also found physical applications in different branches. We mention here the connection of the dimer problem on the hexagonal lattice [6] to commensurate-incommensurate phase transitions due to a domain-wall analogy [7,8]. This also provides us with a model for the Pokrovsky — Talapov phase transition [9]. The second line of interest arises from the RVB theory of high-T_c superconductivity [10—12]. The classical dimer model is here a structural ingredient of the theory to describe the short range resonating valence bond state [11,12]. The important feature of the dimer model is its fermionic nature. Kasteleyn [1,6] used combinatorial argu-

*Max Planck Institut für Festkörperforschung, 7000 Stuttgart 80, Germany

ments to show that the statistical sum of dimer problems can be expressed in terms of Pfaffian forms. In retrospection, this already suggests the fermionic nature of the problem. The combinatorial fermionic analysis of the problem has been performed later on by Samuel [13] and Abanov [14]. However, the combinatorial approaches are rather complicated and differ significantly from the methods commonly accepted in solid state physics where the dimer models have found recently important applications.

In this note we present a new constructive solution for the 2D dimer problem based on the Grassmann variable (fermionic) integrals and factorization principles for the density matrix. The approach is straightforward and very simple, combinatorial considerations are not needed. We present the basic ideas of fermionization by an example of the rectangular inhomogeneous lattice. For this lattice, we derive a representation for the partition function in the form of a Gaussian fermionic integral. This means that the dimer model is equivalent to the free fermion field theory on a lattice. The principal point of the solution is the mirror-ordered representation for the dimer density matrix. At this stage we apply the ideas first developed in the context of the 2D Ising model [15].

2. The Closed-Packed Dimer Problem

We consider the closed-packed dimer problem on the inhomogeneous rectangular lattice with free boundary. The lattice sites mn are numbered by discrete Cartesian coordinates $m = 1, 2, ..., M$ and $n = 1, 2, ..., N$ running in horizontal and vertical directions, respectively. The dimers are objects living on lattice bonds. The given bond may be either free or covered by a dimer together with the two adjacent lattice sites. A closed-packed dimer covering is such that each lattice site is occupied by exactly one dimer. The lattice must have even number of sites to be covered completely in a closed-packed fashion since each dimer covers exactly two sites. An example of a closed-packed dimer configuration for a rectangular lattice is shown in Fig.1a. We will associate the horizontal bond $(mn|m+1n)$ and the vertical bond $(mn|mn+1)$ with the site mn, as it is shown in Fig.1c. Let $t^{(1)}_{mn}$ be the weight of the horizontal mn-bond covered by a dimer, analogously we define the weight $t^{(2)}_{mn}$ for the vertical mn-bond, see Fig.1c. The weight of a free bond is 1. The Boltzmann weight of a configuration is the product of the activities $t^{(\alpha)}_{mn}$ ($\alpha = 1,2$) of all occupied bonds and the partition function Q is the sum over all possible closed-packed configurations. This partition function (or generating function in combinatorial interpretation) is the main subject of interest.

The formal combinatorial definition for Q can be put in a more constructive form as follows (also see [16]). With each lattice site mn we associate the commuting nilpotent variable η_{mn} with the property $\eta_{mn}^2 = 0$ and write:

$$Q = \underset{(\eta)}{Sp} \prod_{m=1}^{M} \prod_{n=1}^{N} (1 + t_{mn}^{(1)} \eta_{mn} \eta_{m+1\,n}) (1 + t_{mn}^{(2)} \eta_{mn} \eta_{m\,n+1}), \qquad (1)$$

with the free-boundary conditions: $\eta_{M+1\,n} = \eta_{m\,N+1} = 0$. The averaging over separable η_{mn} variable is here defined as follows:

$$\underset{(\eta_{mn})}{Sp} (1|\eta_{mn}|\eta_{mn}^2|\eta_{mn}^3|\eta_{mn}^4|...) = (0|1|0|0|0|...), \qquad (2)$$

and the total averaging in (1) involves the averagings over η_{mn} at all sites. By multiplication of the factors in the «density matrix» in (1) we get a polynomial in η-variables in which the given η_{mn} variable enters up to the fourth power. To fulfil the closed-packing condition we have to pick up only the terms in which each of the variables η_{mn} is presented in the first power. This is just realized by the selection rules (2). Our goal is now to pass from the commuting variables η to the anticommuting Grassmann variables a with the corresponding change of averaging. The point is that the Grassmann variables are «good» variables, with many plausible properties, and we know how to extract numbers from the Grassmann-variable expressions, which is not the case for the commuting nilpotent η-variables.

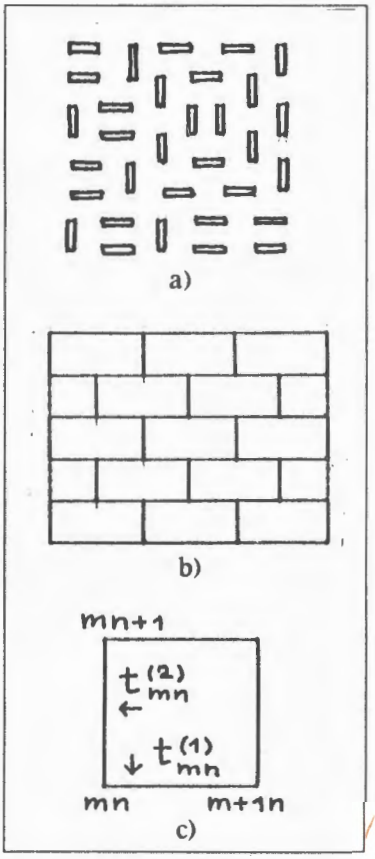

Fig. 1. a) The closed-packed dimer covering for a rectangular lattice. b) A fragment of brick lattice, such a lattice is topologically equivalent to hexagonal lattice. c) Enumeration of sites and bonds on a rectangular cell

3. Grassmann Variables

We remember that the Grassmann variables are classic fermionic numbers purely anticommuting to zero. Given a set of Grassmann variables $a_1,\ldots, a_N$, we have $a_i a_j + a_j a_i = 0$, $a_j^2 = 0$. The Berezin's rules of integration over one variable are [17]:

$$\int da_j \cdot a_j = 1, \quad \int da_j \cdot 1 = 0. \tag{3}$$

In the multidimensional integral the differential symbols $da_1,\ldots, da_N$ are again anticommuting with each other and with the variables. The basic formulas of the Grassmann-variable analysis are for the Gaussian fermionic integrals [17]. The Gaussian integral of the first kind is related to the determinant:

$$\int \prod_{j=1}^{N} da_j^* \, da_j \, e^{\sum_{i=1}^{N}\sum_{j=1}^{N} a_i A_{ij} a_j^*} = \det \hat{A}, \tag{4}$$

here $\{a_j, a_j^*\}$ is a set of completely anticommuting Grassmann variables, the matrix in the exponential is arbitrary. The Gaussian integral of the second kind is related to the Pfaffian form of the skew-symmetric matrix:

$$\int da_N \ldots da_2 da_1 \, e^{\frac{1}{2}\sum_{i=1}^{N}\sum_{j=1}^{N} a_i A_{ij} a_j} = \text{Pfaff}\, \hat{A}, \quad A_{ij} = -A_{ji}. \tag{5}$$

The Pfaffian form is some combinatorial polynomial in elements A_{ij} known in mathematics for a long time [18]. The Pfaffian and determinant of the associated skew-symmetric matrix are algebraically related: $\det \hat{A} = (\text{Pfaff}\, \hat{A})^2$. This relation can be most easily proved in terms of the fermionic integrals like (4) and (5) [13].

Let it be given two Grassmann variables a and a^*. The elementary Gaussian exponential is $e^{\lambda a a^*} = 1 + \lambda a a^*$ (the series terminates since $(aa^*)^2 = 0$). Making use of the basic rules (3), for the complete set of the Gaussian averages we find: $\int da^* da \, e^{\lambda a a^*} \{1, a, a^*, aa^*\} = \{\lambda, 0, 0, 1\}$. Note that the linear terms give zero result as a consequence of $\int da_j \cdot 1 = 0$. We can then factorize the typical dimer weight in (1) as follows:

$$1 + t\eta\eta' = \int da^* da \, e^{aa^*} (1 + ta\eta)(1 + a^*\eta'). \tag{6}$$

We will apply the factorization like (6) in order to pass in (1) from the commuting η-variables to the anticommuting Grassmann variables.

4. Fermionization

We first factorize the local weights from (1) following (6). To this end, we introduce a set of purely anticommuting Grassmann variables $\{a_{mn}, a^*_{mn}, b_{mn}, b^*_{mn}\}$, a pair per bond, are write:

$$1 + t^{(1)}_{mn}\eta_{mn}\eta_{m+1\,n} = \int da^*_{mn} da_{mn}\, e^{a_{mn}a^*_{mn}} \times$$

$$\times (1 + t^{(1)}_{mn}a_{mn}\eta_{mn})(1 + a^*_{mn}\eta_{m+1\,n}) = \underset{(a_{mn})}{Sp}\, A_{mn}A^*_{m+1\,n}, \qquad (7a)$$

$$1 + t^{(2)}_{mn}\eta_{mn}\eta_{m\,n+1} = \int db^*_{mn} db_{mn}\, e^{b_{mn}b^*_{mn}} \times$$

$$\times (1 + t^{(2)}_{mn}b_{mn}\eta_{mn})(1 + b^*_{mn}\eta_{m\,n+1}) = \underset{(b_{mn})}{Sp}\, B_{mn}B^*_{m\,n+1}, \qquad (7b)$$

where we introduced the abbreviated notation for the arising Grassmann factors:

$$A_{mn} = 1 + t^{(1)}_{mn}a_{mn}\eta_{mn}, \quad A^*_{m+1\,n} = 1 + a^*_{mn}\eta_{m+1\,n},$$

$$B_{mn} = 1 + t^{(2)}_{mn}b_{mn}\eta_{mn}, \quad B^*_{m\,n+1} = 1 + b^*_{mn}\eta_{m\,n+1}, \qquad (8)$$

and by Sp we denote Gaussian averagings like $\int da^* da\, e^{aa^*}(...)$ and $\int db^* db\, e^{bb^*}(...)$ as is clear from above. Note that the indices mn of the Grassmann factors in (7)—(8) are chosen to be equal to the mn indices of the η-variables involved in the corresponding factors.

There are in general the four factors $A_{mn}, A^*_{mn}, B_{mn}, B^*_{mn}$ with a given index mn, which all involve the same variable η_{mn} associated with the mn-site of the lattice. The idea is to group together the four factors with the same η_{mn}-variable and to perform the η-averaging in each group of factors independently. The obstacle is that separable factors (8) are neither commuting, nor anticommuting with each other. Thus we have to make a special consideration of ordering in the products of noncommuting factors.

To solve this problem, we will use a special arrangement of the Grassmann factors. The two main principles are illustrated here by tutorial examples:

$$(x_0\bar{x}_1)\,(x_1\bar{x}_2)\,(x_2\bar{x}_3)\,(x_3\bar{x}_4) = x_0(\bar{x}_1x_1)\,(\bar{x}_2x_2)\,(\bar{x}_3x_3)\,\bar{x}_4, \tag{9}$$

and

$$(x_1\bar{x}_1)\,(x_2\bar{x}_2)\,(x_3\bar{x}_3) = (x_1(x_2(x_3\bar{x}_3)\,\bar{x}_2)\,\bar{x}_1) = x_1x_2x_3\cdot\bar{x}_3\bar{x}_2\bar{x}_1. \tag{10}$$

In (9) we simply reread the product by joining the factors with the same index. In (10) we assume that the doublets $x_j\bar{x}_j$ are totally commuting with any separable factors though the factors themselves may be noncommuting with each other.

We must prepare such an expansion of the dimer density matrix into the product of the noncommuting factors (8) that it is possible to perform the η_{mn}-averaging at each site. To this end, the Grassmann factors with given mn are to be placed nearby in the process of averaging over η_{mn}. What can be used in the ordering arrangements is that the doubled factors $A_{mn}A^*_{m+1\,n}$ and $B_{mn}B^*_{m\,n+1}$ presenting the bond weights in (7) can be considered as totally commuting objects, if taken as a whole, under the sign of the Gaussian averaging. We thus may move symbols $A_{mn}A^*_{m+1\,n}$ and $B_{mn}B^*_{m\,n+1}$ through any product of other Grassmann factors. With these notes we now directly proceed to the construction of a suitable factorized representation for the density matrix. In the forthcoming transformations from (11) to (13) we omit for brevity the symbol of the Gaussian averaging on the right-hand sides.

First, putting one weight between the two Grassmann factors of another, we write:

$$(1 + t^{(1)}_{mn}\eta_{mn}\eta_{m+1\,n})\,(1 + t^{(2)}_{mn}\eta_{mn}\eta_{m\,n+1}) =$$

$$= B_{mn}A_{mn}A^*_{m+1\,n}B^*_{m\,n+1}. \tag{11}$$

Next, we fix n and multiply the factors over m applying the rules (9) and (10):

$$\prod_{m=1}^{M}(1 + t^{(1)}_{mn}\eta_{mn}\eta_{m+1\,n})\,(1 + t^{(2)}_{mn}\eta_{mn}\eta_{m\,n+1}) =$$

$$= \prod_{m=1}^{M}\left\{B_{mn}A_{mn}A^*_{m+1\,n}|B^*_{m\,n+1}\right\} =$$

$$= \prod_{m=1}^{M} \overrightarrow{B_{mn} A_{mn} A^*_{m+1\,n}} \cdot \prod_{m=1}^{M} \overleftarrow{B^*_{m\,n+1}} =$$

$$= \prod_{m=1}^{M} \overrightarrow{A^*_{mn} B_{mn} A_{mn}} \cdot \prod_{m=1}^{M} \overleftarrow{B^*_{m\,n+1}}, \qquad (12)$$

where the arrows indicate the directions of increasing m in the ordered products. In the last line we have taken into account that $A^*_{M+1\,n} = 1$ due to the boundary condition $\eta_{M+1\,n} = 0$, also see the definition of factors in (8). And, on the contrary, on the left end of the ordered product in (12) we introduced, formally, the lacking factors A^*_{1n} in which we put $a^*_{0n} = 0$, so that in fact $A^*_{1n} = 1$.

In turn, we now multiply the products (12) with respect to index n, with n increasing from left to right, and applying (9):

$$\prod_{n=1}^{N} \left\{ \prod_{m=1}^{M} \overrightarrow{A^*_{mn} B_{mn} A_{mn}} \cdot \prod_{m=1}^{M} \overleftarrow{B^*_{m\,n+1}} \right\} =$$

$$= \prod_{n=1}^{N} \left\{ \prod_{m=1}^{M} \overleftarrow{B^*_{mn}} \cdot \prod_{m=1}^{M} \overrightarrow{A^*_{mn} B_{mn} A_{mn}} \right\}, \qquad (13)$$

where in the final expression we again annihilate factors $B^*_{m\,N+1} = 1$ and create factors $B^*_{m1} = 1$ with $b^*_{m0} = 0$, analogously to the boundary transformations in (12). In fact, being forced in (12) to separate the mn and $m\,n+1$ Grassmann factors in order to apply the linear arrangement (9) with respect to m, in (13) we are trying to restore the normal state by gathering the factors with equal values of mn into separable groups.

For the dimer partition function (1) we thus come to the following factorized representation:

$$Q = \underset{(\eta|a,b)}{Sp} \prod_{n=1}^{N} \left\{ \prod_{m=1}^{M} \overleftarrow{B^*_{mn}} \cdot \prod_{m=1}^{M} \overrightarrow{A^*_{mn} B_{mn} A_{mn}} \right\}, \qquad (14)$$

where we have restored the sign of the total Gaussian averaging over the fermionic variables. Note that the original free-boundary conditions for the η-variables have now been transformed into the free-boundary fermionic conditions in (14). The η-averaging can be readily performed in representation (14).

The η-averaging reduces to the averaging over separable variables η_{mn} at the junction of the m-products in (14) and yields, finally, the product of the linear forms:

$$L_{mn} = t^{(1)}_{mn} a_{mn} + t^{(2)}_{mn} b_{mn} + a^*_{m-1\,n} + (-1)^{m+1} b^*_{m\,n-1}. \qquad (15)$$

We first fix n and perform the η-averaging at the junction for $m = 1,2,..., M$, and all over again for other values of n. At the first step, $m = 1$, we average the product $B^*_{mn} A^*_{mn} B_{mn} A_{mn} = 1 + \eta_{mn}(t^{(1)}_{mn} a_{mn} + t^{(2)}_{mn} b_{mn} + a^*_{m-1\,n} + b^*_{m\,n-1}) + ...$ with the result (15). Then we move the fermionic form L_{mn} from the junction to the left through the remaining product of B^*_{mn} factors, this explains the appearance of the $(-1)^{m+1}$ factor in (15) in the general case. The η-variables being eliminated, the partition function is the product of the forms L_{mn} under the Gaussian fermionic averaging coming from (14). To bring this expression into a more convenient form, we exponentiate the factors L_{mn} introducing auxiliary Grassmann variables c_{mn} and making use of the identity $L_{mn} = \int dc_{mn}\, e^{c_{mn} L_{mn}}$. This gives:

$$Q = \int \prod_{n=1}^{N} \prod_{m=1}^{M} da^*_{mn} da_{mn} db^*_{mn} db_{mn} \overrightarrow{dc_{mn}} \times$$

$$\times \exp\left\{ \sum_{m=1}^{M} \sum_{n=1}^{N} [a_{mn} a^*_{mn} + b_{mn} b^*_{mn} + c_{mn} L_{mn}] \right\}, \qquad (16)$$

with $a^*_{0n} = 0$, $b^*_{m0} = 0$. We have in (16) the fermionic Gaussian integral. This expression can in turn be simplified by integrating out the a- and b-fields by using the identity $\int da^* da\, e^{aa^* + aL' + a^* L''} = e^{L'' L'}$, which follows from the basic rules (3), here L', L'' are some linear forms in c-variables. The remaining integral is:

$$Q = \int \prod_{n=1}^{N} \prod_{m=1}^{M} \overrightarrow{dc_{mn}} \times$$

$$\times \exp\left\{ \sum_{m=1}^{M} \sum_{n=1}^{N} \left[t^{(1)}_{mn} c_{m+1\,n} c_{mn} + (-1)^{m+1} t^{(2)}_{mn} c_{m\,n+1} c_{mn} \right] \right\}, \qquad (17)$$

with free-boundary conditions for the c-variables, $c_{M+1\,n} = 0$, $c_{m\,N+1} = 0$. This is the final exact representation for the partition function of the closed-packed inhomogeneous dimer model disposed on a finite rectangular lattice with free boundary. This expression is completely equivalent to the original representation of eq. (1). The partition function is now expressed as a simple fermionic Gaussian integral. In the field theoretical language the quadratic fermionic form in the exponential is called fermionic action. Since the action is quadratic, we deal here with the free fermion theory for the dimer model.

5. Discussion

The Gaussian representation (17) is our main result. As it follows from (5), the integral (17) defines a Pfaffian form, this fact is in accordance with the Kasteleyn analysis of dimer combinatorics [1]. We stress however that we have simply calculated (17) in a formal way, without using any combinatorial considerations.

It is important that the fermionic representation (17) is obtained in the most general case of an inhomogeneous distribution of the dimer weights. This can be used at least for three purposes: (i) one can express the dimer-dimer correlation functions simply by differentiating (17) with respect to the local weights $t^{(\alpha)}_{mn}$, (ii) one can study the disordered problem or the influence of impurities, and (iii) one can consider in a simple way problems with a complicated structure of the elementary cell. We also note that the representation (17) contains all the information about the brick lattice, see Fig.1b, which is equivalent to the hexagonal lattice neglecting the boundary effects. The fermionic representation for Q for the brick-hexagonal lattice arises simply by making zero some of the vertical weights $t^{(2)}_{mn}$ in accordance with Fig.1b. It is interesting that the homogeneous hexagonal lattice exhibits an exotic phase transition [6—8] as distinct from the homogeneous rectangular lattice with no phase transition. Eq. (17) thus preserves the information about partition functions and correlations in homogeneous rectangular and hexagonal lattices and may be a good starting point also for further studies.

For actual calculations for homogeneous lattices, the standard device is to pass to the momentum space (Fourier transformation for fermions). Let us illustrate this for the rectangular lattice. In the homogeneous case, $t^{(1)}_{mn} = t_1$ and $t^{(2)}_{mn} = t_2$, the fermionic action in (17) can be put to block-diagonal form by the substitution:

$$c_{mn} = \frac{2i^{m+n}}{\sqrt{(M+1)(N+1)}} \sum_{p=1}^{M} \sum_{q=1}^{N} c_{pq} \sin \frac{\pi pm}{M+1} \sin \frac{\pi qn}{N+1}. \qquad (18)$$

Let both M and N be even. The partition function then appears in the form (momentum space representation):

$$Q = \int \prod_{q=1}^{N} \prod_{p=1}^{M} \overset{p}{dc_{pq}} \exp \sum_{p=1}^{\frac{1}{2}M} \sum_{q=1}^{\frac{1}{2}N} \left\{ 2it_1 \cos \frac{\pi p}{M+1} \times \right.$$

$$\times (c_{pq} c_{M+1-p\,N+1-q} + c_{p\,N+1-q} c_{M+1-pq}) + 2it_2 \cos \frac{\pi q}{N+1} \times$$

$$\left. \times (c_{pq} c_{p\,N+1-q} + c_{M+1-pq} c_{M+1-p\,N+1-q}) \right\}. \qquad (19)$$

The pq sum in (19) is reduced to a half-interval $\frac{1}{2}M, \frac{1}{2}N$ when we select explicitly and join together all the terms including the variables c_{pq}, $c_{M+1-p\,q}$, $c_{p\,N+1-q}$, $c_{M+1-p\,N+1-q}$. We thus have to integrate separately over the groups of variables c_{pq}, $c_{M+1-p\,q}$, $c_{p\,N+1-q}$, $c_{M+1-p\,N+1-q}$. Evaluation of the integral gives:

$$Q = \prod_{p=1}^{\frac{1}{2}M} \prod_{q=1}^{\frac{1}{2}N} \left[4t_1^2 \cos^2 \frac{\pi p}{M+1} + 4t_2^2 \cos^2 \frac{\pi q}{N+1} \right], \qquad (20)$$

in accordance with the combinatorial result [1,2].

The fermionization procedure can also be performed, as a generalization of the treatment exposed above for the free boundary, for the toroidal (periodic in both directions) boundary conditions for the inhomogeneous rectangular lattices. We refer here to the experience with the 2D Ising model [19]. Not going into the detail, the final result is:

$$Q|_{\text{torus}} = \frac{1}{2} [G|_{--} + G|_{-+} + G|_{+-} - G|_{++}], \qquad (21)$$

where the fermionic integral G is the integral (17), but now we have the four different combinations of the aperiodic-periodic closing conditions for fermions: $(\pm|\pm) = (c_{M+1\,n} = \pm c_{1n} | c_{m\,N+1} = \pm c_{m1})$. In the homogeneous case $t_{mn}^{(\alpha)} = t_\alpha$, the four integrals in (21) can again be evaluated explicitly, reproducing in a simple way the result of complicated combinatorial analysis [1].

Note that putting $t_1 = t_2 = 1$ in (20), or in the corresponding analytic expression given by (21) in the homogeneous case, we simply get the number of the dimer configurations on the corresponding lattices. Fisher [20] has evaluated, as illustration, the number of all possible coverings of the checkerboard by dominos, which appears to be $N_F = 12988816$ (this number is given by (20) with $M = N = 8$ and $t_1 = t_2 = 1$). We have evaluated the analogous number for the checkerboard swept into a torus. The torus number appears to be significantly larger, $N_T = 311853312$.

In conclusion, we have reformulated the closed-packed dimer problem on the inhomogeneous 2D lattice as a free fermion field theory. The partition function is obtained in the form of a Gaussiann Grassmann-variable integral. This puts the dimer problem, which is originally a combinatorial problem, more close to the typical models of quantum statistics and solid state physics with the opportunity to apply the well developed field-theoretical methods. In the homogeneous cases fermionization yields exact analytic solutions for thermodynamic functions and correlations. The fermionization procedure can as well be applied to more complicated dimer like problems equivalent to non-Gaussian fermionic theories. Grassmann variables are the powerful tool for studying dimer-type models.

This work was supported by the Heisenberg-Landau Program.

References

1. Kasteleyn P.W. — Physica (Utrecht), 1961, 27, p.1209.
2. Temperley H.N.V., Fisher M.E. — Phil. Mag., 1961, 6, p.1061.
3. Mc Coy B.M., Wu T.T. — The Two-Dimensional Ising Model, Harvard U.P., Cambridge, 1973.
4. Montroll E.W. — In: Applied Combinatorial Mathematics, Ed. E.F.Beckenbach, John Willey, New York, 1964.
5. Priezzhev V.B. — Usp. Fiz. Nauk, 1985, 147, p.747; Sov. Phys. Usp., 1985, 28, p.1125.
6. Kasteleyn P.W. — J. Math. Phys., 1963, 4, p.287.
7. Bhattacharjee S.M., Nagle J.F., Huse D.A., Fisher M.E. — J. Stat. Phys., 1983, 32, p.361.
8. Nagle J.F., Yokoi C.S.O., Bhattacharjee S.M. — In: Phase Transitions and Critical Phenomena, Eds. C.Domb and J.L.Lebowitz, vol.13, Academic Press, London, 1990.
9. Pokrovsky V.L., Talapov A.L. — Phys. Rev. Lett., 1979, 42, p.65.
10. Anderson P.W. — Science, 1987, 235 , p.1196.

11. Fradkin E. — Field Theories of Condensed Matter Systems, Addison-Wesley, Redwood City C.A., 1991.
12. Sutherland B. — Phys. Rev., 1988, B37, p.3786.
13. Samuel S. — J. Math. Phys., 1980, 21, p.2806.
14. Abanov A.G. — Zh. Eksp. Teor. Fiz., 1992, 101, p.1937; Sov. Phys. JETP, 1992, 74, p.1036.
15. Plechko V.N. — Doklady Acad. Nauk SSSR, 1985, 281, p.834; Sov. Phys. Dokl., 1985, 30, p.271.
16. Fradkin E.S., Shteingradt D.M. — Preprint FIAN No.98, Moscow, 1980.
17. Berezin F.A. — The Method of Second Quantization, Academic Press, New York, 1966.
18. Caianiello E.R. — Nuovo Cim. Suppl., 1959, 14, p.177.
19. Plechko V.N. — Teor. Mat. Fiz., 1985, 64, p.150; Theor. Math. Phys., 1985, 64, p.748.
20. Fisher M.E. — Phys. Rev., 1961, 124, p.1664.

Received on June 29, 1993.

УДК 539.211 + 541.183.26

THE DYNAMICS OF SORPTION OF INTERACTING PARTICLES

V.K.Fedyanin

Specific features of particles transport when their sorption is taken into account by the surface are analyzed: flows of gas or liquid in systems of different geometry; (for definiteness, the formulae are given for the flow through a tube of length L). An activated complex is treated as an admixture. The quantum statistical Hamiltonian of adsorption is taken as an effective Hamiltonian of an open system. The kinetic equation of sorption, except for the case of Henry's isotherm, is essentially nonlinear in coverage, which provides a high degree of nonlinearity for differential equations and concentration of particles in the flow. Solutions for Henry's isotherm and the asymptotics of solutions for the wave front of Langmuir's isotherm are analytically analyzed. It is important to take into account an interaction in the adsorbate, and for chemisorption it allows one to show that starting from some coverages desorption dominates over adsorption. This is especially essential for dissociative adsorption ($A_n \rightarrow n[A]^4$). Certain relations between the interaction of adatoms and adatoms with the activated complex may lead to the formation of chemical waves of concentration in the flow and appearance of strange attractors.

The investigation has been performed at the Laboratory of Theoretical Physics, JINR.

Динамика сорбции взаимодействующих частиц

В.К.Федянин

Исследуется влияние активной поверхности на поток газа или жидкости через среду различной геометрии (формулы приведены для потока через трубу длины L радиуса R_0). Активные комплексы поверхности рассматриваются как примеси. При анализе используется эффективный квантовостатистический гамильтониан открытой системы адсорбат — адсорбент. Для всех изотерм адсорбации, кроме изотермы Генри, кинетические уравнения сорбции существенно нелинейны, что обуславливает высокую нелинейность концентрации в потоке. Аналитически проанализирована адсорбция Генри и, в приближении фронта волны, Ленгмюра. Учет взаимодействия в адсорбате позволяет сделать вывод, что, начиная с определенных покрытий десорбция превалирует над адсорбцией. Это весьма существенно для диссоциативной хемисорбции ($A_n \rightarrow n[A]$)^4. При определенных соотношениях взаимодействий между адатомами и адатомами с активными центрами возможно возникновение автоволн концентрации и странных аттракторов.

Работа выполнена в Лаборатории теоретической физики ОИЯИ.

The quantum statistical Hamiltonian of absorption is taken as an effective Hamiltonian of an open system

$$H = -\nu \sum_f N_f - \varepsilon \sum_{\langle fg \rangle} N_f N_g. \qquad (1)$$

Here ε is an effective parameter of the interaction ($\varepsilon \sim 0.05$ eV for the physical adsorption, often $\varepsilon > 0$, $|\varepsilon| \sim 0{,}1 + 0{,}2$ for the chemical adsorption, that is, $\varepsilon < 0$; ν is an effective chemical potential of the system adsorbat-adsorbent, defined by the chemical potential of the adatom of the open system $\mu(A_n)$: $\mu(A_n) = n\mu[A]$, and by the characteristics of the adsorbent-adsorbat system [1]. For dissociative adsorption we take the gas $A_n \to n[A]$

$$\nu = k_B T \left[p_0 \frac{\exp \beta(\varepsilon_0 + \delta\mu_e) \cdot J_a^n}{k_B T J_0(\beta)} \right]^{1/n} = k_B T (a p_0)^{1/n}, \qquad (2)$$

a is the coefficient of the adsorption, p_0 is the equilibrium of the pressure for the coverage $\theta = \theta(p_0, T/\varepsilon..) = \langle N_f \rangle$, ε_0 is the binding energy of the adatom, J_a, J_0 are the partition functions of the adatom and of the particle for a gas, $\delta\mu_e$ is the change of the chemical potential of the electronic subsystem [2], T is the temperature, k_B is the Boltzmann constant. In the equation (1) $N_f = 0.1$ ($N_f = 0$ is the case of the open sites; $N_f = 1$, of the packing sites, and the summation is carried out over all adsorption sites on the surface (f) and out over all ($g = 1,2,...,z$) sites (f,g). The Hamiltonian (1) may be deduced from the first principles in the framework of an Anderson-Ising composite model [3]. Within the composite Hamiltonian method the coverage dependence of the chemisorption characteristic for a single hydrogen-like adatom on the transition metal surface like the chemisorption energy, ε_0 changes of the Fermi level $\delta\mu_e$, the electric charge $e[1 - \bar{n}_{f\uparrow} - \bar{n}_{f\downarrow}]$ and $\mu_e[1 - \bar{n}_{f\uparrow} - \bar{n}_{f\downarrow}]$ magnetic moment at adsorbed atoms are investigated [2]; $\bar{n}_{f\sigma} = \langle N_{f\sigma} n_{f\sigma} \rangle_M \cdot \theta^{-1}$, $n_{f\sigma} = a^+_{f\sigma} a_{f\sigma}$. The unusual form of the average $\bar{n}_{f\sigma}$ arises from the fact that the configuration of adatoms is not fixed and the electronic correlation function $\bar{n}_{f\sigma}$ should be interpreted as the probability of finding an electron with the spin $\sigma = \pm 1/2$ at the adsorption center «f» when the latter is already occupied.

This fact is discussed in detail in [2,3]. We should remark that ε_0, $|\varepsilon|$ weakly depend on θ and T.

If for the calculation of the equilibrium characteristics of the adsorption important are $\langle N_f \rangle$, $\langle N_f N_g \rangle$, for the calculation of the adsorption and desorption rates we must have the correlation functions $F_k(\theta) = \langle N_f \prod_1^k N_g \rangle$, $k = 1,...,z$ for the one-site adsorption [4] and $F_k^{(h)} = \langle N_f \prod N_g \prod N_k \rangle$, $k = 1,...,z$, j are the numbers for the next-neighbour sites [5] for dissociative two-site adsorption.

The kinetic equation of sorption (for simplicity we take the case of the one-site adsorption) has the form [4]

$$\partial_t \theta = V_{ads} - V_{des}$$

$$V_{ads} = r_A F(\theta), \quad V_{des} = r_D F(\theta)$$

$$F(\theta) = \sum_{k=0}^{z} \frac{x^k}{k!} F_k(\theta), \quad x = \exp[\beta(\varepsilon_1 - \varepsilon)] - 1$$

$$r_A = \frac{J^* P \exp[-\beta(\varepsilon_k - \tilde{\varepsilon}_0)]}{J_0 h \sigma a p_0}, \quad r_D = \frac{J^* \exp(-\beta \varepsilon_k)}{J_a h \beta \sigma}, \tag{3}$$

J^*, ε_k is the partition function and the energy of an activated complex, P is the pressure in the system, ε_1 is the interacting energy of the adatom with an activated complex; $\tilde{\varepsilon}_0 = \varepsilon_0 + \delta \mu_e$. The $F(\theta)$ is some function of the coverage θ. The expressions V_{ads} and V_{des} for dissociative adsorption are taken from [5]. The difference between r_A and r_D lies in that the activated complex of the adsorption is in equilibrium with the gas molecules; and of the description activated complex, with the adatoms.

There is the equation of the transfer. For the gas sorption we have the equation (with the diffusion)

$$\partial_t \theta + \partial_t \nu = -V_0 \partial_x \nu + D \partial_{xx} \nu, \tag{4}$$

V_0 is the velocity, D is the coefficient of the diffusion.

There are initial and boundary conditions:

$$\nu(x,0); \ \dot{\nu}(x,0); \ \nu(0,t) \equiv \nu_0(t), \ \dot{\nu}(0,t) = \dot{\nu}_0(t). \tag{5}$$

For the ideal gas, $P = \dfrac{n(x,t)R_A T)}{V}$, $n(x,t)$ is the number of the mol. on the place «x» and on the time «t»,

$$\nu(x,t) = u(x,t)\frac{V_0}{\Delta}, \quad u(x,t) = \frac{n(x,t)N_A}{V}, \tag{4'}$$

V_0 is the volume of the gas molecule; Δ, a geometrical factor; $\Delta \sim \dfrac{2}{3}\dfrac{1 - d/R_0)}{(1 - d/D)}$ is the same effective parameter of the adsorption region, d, $D = 2R_0$, R_0 is the radius of the tube. The parameter μ^{-1} has the dimension of the time

$$\partial_t \theta = \mu\left[\frac{P \cdot a}{P_0 \cdot a} - 1\right] F(\theta), \quad \mu = \frac{k_B T J^* \exp(-\beta\varepsilon_k)}{\sigma h J_a} \tag{6}$$

and can be «a chemical time».

In the self-consistent approximation [4,6] we have for the equation (6)

$$\frac{1}{ap_0} = \frac{1 - \theta)}{\theta}\exp(\beta\, z\, \varepsilon\, \theta), \quad F(\theta) = \theta(1 + x\theta)^z$$

$$\partial_t \theta = \tau_0^{-1}[(1 - \theta)\cdot\nu \ \exp(\beta\, z\, \varepsilon\, \theta) - \delta\cdot\theta\,](1 + x\,\theta)^z$$

$$\tau_0 = \frac{\sigma h J_0 \nu_0}{k_B T J^* \Delta} \exp[-\beta(\tilde{\varepsilon}_0 - \varepsilon_k)], \quad \delta = \frac{V_0 J_0}{\Delta J_a}\exp(-\beta\tilde{\varepsilon}_0), \tag{7}$$

z is the number of the sites ($z = 3.4.6$). The r_0 can be called «an adsorption time». From the physical point of view $\delta << 1$. When $\varepsilon = \varepsilon_1$ and for the case of Henry's isotherm ($\nu << 1, \theta << 1$) we have

$$\partial_t \theta = \tau_0^{-1}(\nu - \delta\,\theta),$$

$$\partial_t \theta + \partial_t \nu = -V_0 \partial_x \nu + D\partial_{xx}\nu, \ \nu(0,t) = \nu_0(t). \tag{8}$$

The case of Langmuir's isotherm ($\varepsilon = \varepsilon_1 = 0, \ 0 \le \theta \le 1$) we have

$$\partial_t \theta = \tau_0^{-1}[1 - \theta)\cdot\nu - \delta\cdot\theta\,],$$

$$\partial_t \theta + \partial_t \nu = -V_0 \partial_x \nu + D\partial_{xx}\nu, \ \nu(0,t) = \nu_0(t), \tag{9}$$

The kinetic equation (7) is essentially nonlinear in coverage, which provides a high degree of nonlinearity for differential equations and concentration of particles in the flow.

Solutions for Henry's isotherm and the asymptotics of solutions for the wave front of Langmuir's isotherm [7]

$$\tau = t - \frac{x}{V_0}, \quad \sigma = \frac{x}{V_0} \tag{10}$$

with the help of the Laplace transformation are analytically analyzed. In the last case we can introduce the «potential function» $\psi(x,t)$ and by the

$$\nu = \partial_\tau \psi, \quad \theta = -\partial_\sigma \psi \tag{11}$$

and Koul-Hopf like operation

$$\psi = \tau_0 \ln \chi(x,t). \tag{12}$$

we obtaine for the Langmuir's case the equation

$$\chi_{\tau\sigma} + \tau_0^{-1}\chi_\tau + \mu\chi_\sigma = 0. \tag{13}$$

For the case of the (x,t)-variables

$$\frac{\tau_0}{1+\delta}[\chi_{tt} + V_0\chi_{tx}] + \chi_t + V_0\frac{\delta}{1+\delta}\chi_x = 0. \tag{14}$$

For the hyperbolic equation of second order (14) we have the succession of times

$$\tau_1 < \tau_0 < \tau_2, \quad \tau_1 = \frac{\tau_0}{1+\delta}, \quad \tau_2 = \frac{\tau_0}{\delta(1+\delta)}. \tag{15}$$

The «wave of the second order» transfer of the initial profile with the velocity V_0

$$\chi_2(x,t) = \chi_0(\tau)\exp\left(-\frac{x}{\tau_2 V_0}\right). \tag{16}$$

For $t >> \tau_1$ there is a «wave of the first order» which has the velocity $V_1 = V_0\frac{\delta}{1+\delta} << V_0$

$$\chi_1(t,x) = \chi_0\left(t - \frac{x}{V_1}\right). \tag{17}$$

Both eq. (16) and eq. (17) can be derived asymptotically by the Laplace-transformation ($s \to \infty$ for eq. (16) and $t >> \tau_1$ for eq. (17)).

It is important to take into account an interaction in the adsorbate, and for the chemisorption ($\varepsilon < 0$) it follows one to show that starting from some coverages desorption dominates over adsorption. This is especially essential for dissociative adsorption ($A_n \rightarrow n[A]$, O_2; for O_2, H_2, N_2 «n» equals two). For the chemisorption of the interacting adatoms in eq.(7) $\exp(\beta z \varepsilon \theta) \equiv \equiv \exp(-\beta z|\varepsilon|\theta)$ and $\beta z|\varepsilon| \cong 15 \div 25$ for typical systems adsorbat-adsorbent [1].

Certain relations between the interaction of adatoms and adatoms with the activated complex may lead to the formation of chemical waves of the concentration in the flow and appearance of strange attractors for $(r_0)_+ \rightarrow 0$ (maybe it is a case of physical adsorption). From this point of view we must analyse the equation

References

1. Fedyanin V.K. — In: «Trudy I Vsesoyuznoya konferentscii po teorii zhidkosti», LGU, 1972, p.27—41; Particles and Nuclei, 1978, v.9, 4, p.658—695. (in Russian). (There are all the references to may works on the theory of the adsorption, which I have doing in the 1968—1977 years).
2. Cardenas R., Gavrilenko G.M., Fedyanin V.K. — Surf. Sci., 1989, 217, p.468.
3. Gavrilenko G.M. — Physica A, 1988, 150, p.137—158.
4. Fedyanin V.K. — Chem.Phys.Lett., 1973, v.22, 1, p.99;
   Fedyanin V.K., Tovbin Yu.K. «Kinetica hemisorptsia v sisteme vzaimodeistvuyishich chastic I. (in Russian)», Kinetika i Kataliz, 1978, 19, 4, p.989.
5. Fedyanin V.K., Tovbin Yu.K. — Kinetica i Kataliz. 1978, 19, 5, p.1202, (in Russian).
6. Fedyanin V.K. — «Method korrelyatsionnych funktsi v modeli Izinga» (in Russian), In: «Statisticheskaya fisika i kvantovoya theoria polya», Bogolubov N.N. (ed), Nauka, 1973.
7. Whitham G.B. — «Linear and nonlinear waves». Wiley-Interscience, New York, 1974.

Received on July 13, 1993.

УДК 539.173

CROSS-SECTIONS OF BISMUTH NUCLEI FISSION ON THE SECONDARY BEAM OF ^{6}He

N.K.Skobelev, S.M.Lukyanov, O.B.Tarasov,
A.S.Fomichev, V.M.Shilov, Yu.E.Penionzhkevich,
I.David, V.P.Perelygin, S.I.Mulgin, R.Wolski

The cross-sections for fission of ^{209}Bi induced by secondary beams of ^{6}He and ^{4}He are measured in analogous conditions. There is a good agreement with formerly published data on fission cross sections. In the case of the reaction ^{4}He + ^{209}Bi, the cross-section of the fission of ^{209}Bi induced by ^{6}He are significantly higher than the corresponding α-particle-induced fission cross-section. A large energy shift is observed of the threshold for the fission reaction ^{6}He + ^{209}Bi in comparison with the reaction ^{4}He + ^{209}Bi. The analysis of different factors which might be responsible for the observed effect in the fission reaction ^{6}He + ^{209}Bi is also presented.

The investigation has been performed at the Flerov Laboratory of Nuclear Reactions, JINR.

Изучение сечений деления ядер висмута на вторичном пучке ионов ^{6}He

Н.К.Скобелев и др.

Измерены в аналогичных условиях сечения деления ^{209}Bi на вторичных пучках ^{6}He и ^{4}He. Получено согласие экспериментальных данных по сечению деления ^{4}He + ^{209}Bi. Измеренные сечения деления ^{209}Bi ионами ^{6}He значительно превышают сечения деления α-частицами. Получено смещение порога деления для реакции по ^{6}He + ^{209}Bi по сравнению с реакцией ^{4}He + ^{209}Bi. Анализируются различные аспекты для объяснения наблюдаемых особенностей при делении ^{209}Bi ионами ^{6}He.

Работа выполнена в Лаборатории ядерных реакций им. Г.Н.Флерова ОИЯИ.

1. Introduction

The first experiments on the BEVALAC measuring the interaction cross-section at an energy of 800 MeV/A showed [1] that the structure of nuclei far from stability can be studied by using secondary beams of radioactive nuclei. Later on, at the GANIL, RIKEN, JINR and MSU (Michigan) there was carried out a series of experiments studying the interaction cross-sections, the elastic scattering differential cross-sections,

the fragmentation and electromagnetic dissociation on radioactive beams with energies from 10 MeV/A up to 100 MeV/A [2—6]. Basing on these data there were extracted values of radioactive nuclei radii and was confirmed the hypothesis of neutron halo existence in nuclei of ^{11}Li. At the same time, it is evident that further efforts are necessary to investigate the interactions of ^{6}He, ^{8}He, ^{11}Be and ^{17}B for which the existence of a neutron halo of one or several neutrons is possible. In particular, the hypothesis of the neutron halo existence in the nuclei of ^{6}He is finding its theoretical and experimental grounds [4,7,8]. This fact can lead to a decrease of the Coulomb barrier for the reaction of fusion with ^{6}He nuclei, which in its turn will lead to a growing probability of compound nucleus fission. The large angular momentum, introduced into the compound nucleus of ^{6}He, as compared with ^{4}He, also leads to the decrease of the fission barrier of the product nucleus. On the other hand, the extended distribution of neutron density in a ^{6}He nucleus may cause its disintegration in the heavy nucleus field of the target which will lead to the decrease in the cross section of complete fusion of interacting nuclei and, thus, to a smaller fission probability. From this viewpoint, it is of interest to study the fission or fusion cross section with such an exotic nucleus as ^{6}He.

The present research is an attempt to obtain data on the fission cross sections of astatine-213 and astatine-215 nuclei at the irradiation of bismuth-209 nuclei with a secondary beam of ^{6}He and ^{4}He ions under comparable conditions.

2. Experimental Method

Figure 1 presents a scheme of our experimental facility for the production of secondary beams of ^{6}He and ^{4}He and for the investigation of ^{213}At and ^{215}At nuclei fission by these nuclei.

The primary beam of ^{11}B ions accelerated on the U400 was focussed onto a specially manufactured cooled rotating tantalum target designed to absorb completely ^{11}B ions of an energy of 200 MeV. Separation of the Ta + ^{11}B reaction products and their formation into secondary beams were performed by means of an optical-ion system described elsewhere [9]. To improve the purification of the ^{6}He secondary beam of other particles, an Al degrader, with a thickness of up to 100 μm, was installed between the dipole magnets MT1 and MT2. This brought about a change of particles magnetic rigidity. In this connection, the magnetic rigidity in the second dipole MT2

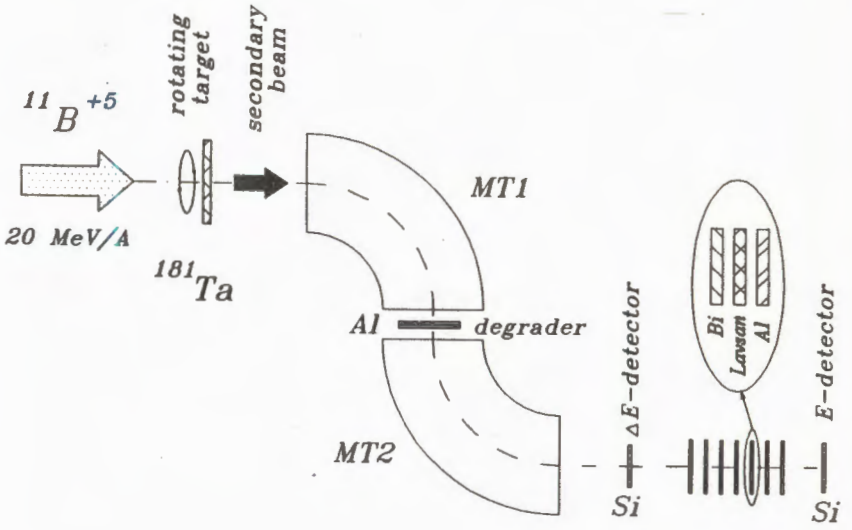

Fig.1. The experimental set-up scheme for the production of secondary beams

was chosen to provide a better ^{6}He or ^{4}He beam purification from other particles. The shaping of the secondary beam, the control of its quality as well as particle monitoring were performed by means of a system of telescopes of $\Delta E \times E$-detectors including surface-barrier detectors of the ΔE-type with thicknesses ranging from 50 to 70 μm and of the E-type with thicknesses reaching 2.5 mm.

Figure 2 shows a typical spectrum of a shaped secondary beam of ^{6}He used in experiments on ^{215}At nuclei fission. The intensity of ^{6}He with an energy of 50 MeV and a resolution of $\cong$ 3% reached 200 pps at a ^{6}He purity of $\cong$ 95%. For the case of a ^{4}He beam used as a secondary beam, the intensity of ^{4}He was limited to several thousands pps, the beam purity at a ^{4}He energy of 54 MeV reached 98%, (the energy resolution $\cong$ 3%). Because of a low intensity of secondary beam particles, a high-efficiency method of registering compound nuclei fission had to be used. For the purpose, special «sandwich-type» arrays (fig.1.) with consecutively alternating targets of ^{209}Bi, polymer plates for registration of fission fragments and additional absorbers made of aluminium were manufactured. Such arrays were installed perpendicularly to the incident beam of secondary particles. The targets were manufactured from bismuth-209 by

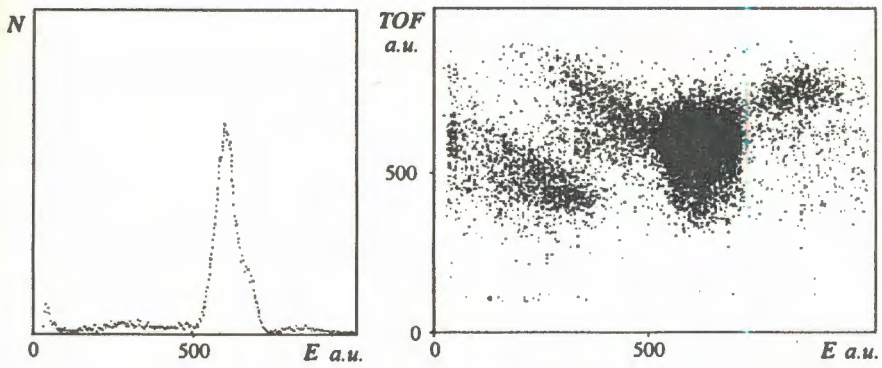

Fig.2. Spectra of shaped secondary beam of ^{6}He used in experiments on fission of ^{213}At and ^{215}At

the method of vacuum sputtering of metallic bismuth onto a 7 μm-thick aluminium backing. Aluminium foils and bismuth targets were tested for uranium contamination by using the neutron-activation method. The analysis showed that the content of uranium in bismuth targets and aluminium backings did not exceed a value of 10^{-7} at/at.

For registration of fission fragments polyterephthalate films $\cong$ 55 μm-thick were chosen. In this case the effective layer of bismuth R_{eff} (mg/cm^2) was determined with the account of the absorption of a part of fragments it brought along [10]. After a 30—48 hours irradiation of an array with a beam of secondary particles the bismuth and aluminium layers were removed and the polyterephthalate was subjected to chemical treatment in NaOH solutions for visual identification of fission fragments. The diameter of fission fragments was increased to 8—10 μm and the search and counting of tracks was performed using a microscope of 100-200 magnification.

We performed also background experiments on fission of Bi targets by a scattered neutron flux. The observed effect of ^{213}At and ^{215}At nuclei fission by nuclei of ^{6}He and ^{4}He could not be explained by fission of uranium admixtures in Bi or by fission of ^{209}Bi nuclei by scattered neutrons.

3. Experimental Results and Discussion

In Figure 3 one can see the observed by us dependencies of fission cross section changes from the energy of bombarding particles (in the center of mass system) ^{6}He and ^{4}He. One can also find there open squares denoting

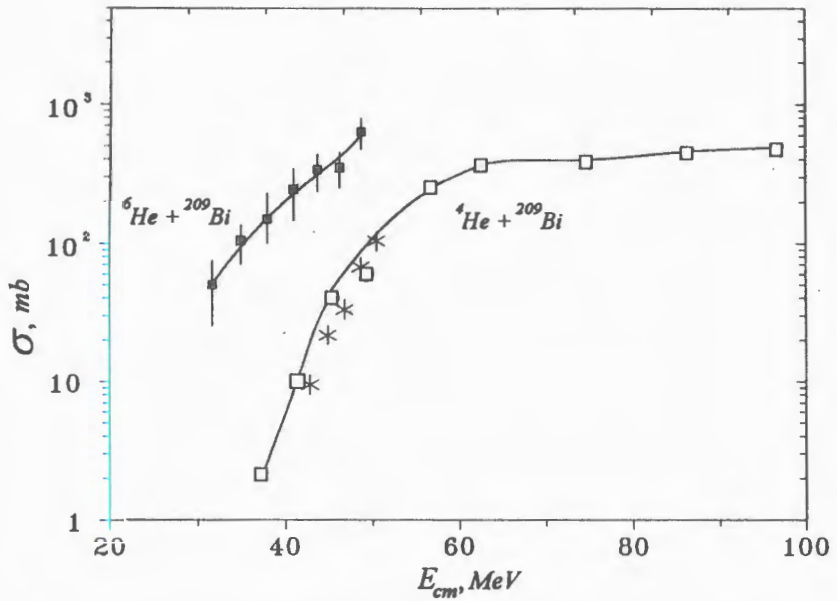

Fig.3. The dependencies of the fission cross sections on the energies of bombarding particles of ^{6}He and ^{4}He (in the c.m.s)

the experimental cross section values of ^{213}At fission by α-particles cited from refs. [11,12].

From the comparison of these data it is well seen that in the case of ^{213}At fission by α-particles (stars) there is a good agreement with the earlier measured values, which is an indication to the correctness of cross section measurements via such a method.

In this connection it is of interest to consider the growth of ^{209}Bi cross section of fission by nuclei ^{6}He as compared with the fission by ^{4}He nuclei. It is evident from the figure that the deviation of the curve for cross sections of nuclei fission by α-particles is substantially greater than the statistical errors.

Of substantial interest is a large energy shift $\cong$ 15 MeV between the thresholds of the reactions ^{4}He + ^{209}Bi and ^{6}He + ^{209}Bi. One can point out at least three reason causing the energy shift in these reactions:

- difference in the Coulomb fusion barriers;
- difference in the fission properties of the produced compound nuclei of ^{213}At and ^{215}At;
- difference in the angular momenta introduced into the compound nucleus at the same incident ion energy in the c.m.s.

3.1. Difference in the Coulomb Barriers of Fusion

As it follows from ref. [13], in the sub-barrier region and near the fusion barrier a considerable growth of fusion cross section is expected for the case of an interaction with neutron-rich nuclei. Here the repulsion potential covers greater distances than in stable nuclei and, as a consequence, the Coulomb barrier between the nuclei with a halo can be lower than between stable partners. The excitation of a soft giant mode at this interaction also assists fusion [4]. Calculations of such effects are very labour-consuming and for the time being we are not able to give quantitative estimation.

There were considered several standard parameterizations for the nuclear part of the ion-ion potential which were suggested in different papers. All of them give close values for the nuclei considered and for our numerical calculations we have used the potential suggested in ref. [22]. For the Coulomb barrier in these reactions there was obtained $V_b = 20.6$ MeV for the reaction ^{4}He + ^{209}Bi and $V_b = 20$ MeV for the reaction ^{6}He + ^{209}Bi. It can be seen that the difference in the Coulomb barriers is too small to explain the energy shift.

Experimental data on the cross sections of fission were obtained at the energies substantially greater than the Coulomb barrier that is why in this energy region one can disregard the coupled-channel effects.

3.2. Account of Compound Nuclei Properties

The full fusion cross section of two spinless nuclei in terms of partial waves can be written down as follows:

$$\sigma_{fus}(E) = \sum_{l=0}^{\infty} \sigma_l(E) = \frac{\pi}{k^2} \sum_{l=0}^{\infty} (2l+1) T_l(E). \qquad (1)$$

In reactions of two nuclei complete fusion, partial penetrations σ_l determine the spin population of a compound nucleus and the competition between particle evaporation channels and fission channels.

For nuclei with the initial spins S_1 and S_2 formula (1) will be rewritten in the following way:

$$\sigma_{fus}(E) = \sum_{J}^{\infty} \sigma_J(E) = \frac{\pi}{k^2(2S_1+1)(2S_2+1)} \sum_{l,J} (2J+1) T_l(E) \qquad (2)$$

and the summing up over J is performed in the interval $|S-l| \le J \le |S+l|$ and $S = S_1 + S_2$.

The analysis of the data was performed in the frame of the statistical approach to the description of the compound nucleus decay. In this approximation the total fission cross sections [14] within this approach are described by the expression:

$$\sigma_{fiss} = \frac{\pi}{k^2} \sum_{l=0}^{l_{cr}} (2l + 1) \frac{\Gamma_f(l)}{\Gamma_f(l) + \sum_{\nu} \Gamma_\nu(l)}, \qquad (3)$$

where l_{cr} is the maximum angular momentum above which the probability of the compound nucleus formation is negligibly small; Γ_f, fission width defined, in the main, by the fission barrier B_f and the value of the parameter of level density in the fission channel a_f, Γ_ν are evaporation widths dependent on the binding energy of the ν particle and on the corresponding parameter of level density a_ν. In this approach the main parameters for the description of $\sigma_f(E)$ are the value l_{cr}, the height of the fission barrier B_f and the ratio of density levels a_f / a_ν.

For the calculation of the values Γ_f and Γ_ν there was used the approach of ref. [15] suggesting and grounding a semiphenomenological method of accounting the influence of shell, super fluid and collective effects on the energy dependencies of level densities. At setting the parameters a_f and a_ν there were used the results of ref. [16] where through the analysis of the fission probability of nuclei with $Z = 81—83$ by light particles there had been obtained a value $a_f / a_\nu = 1.03 \pm 0.01$. The B_f of these nuclei were measured experimentally. There are no experimental data on the value of l_{cr} for the interaction of ^{6}He with heavy nuclei that is why there have been used the l_{cr} values calculated by the model [17]. The model has been selected on the assumption that for ^{4}He ions it gives values of σ_{fus} and l_{cr} which are in satisfactory agreement with the values obtained in ref. [16]. In the calculations of the integral cross sections the contribution of the post-emission fission is taken into account by means of the method presented in ref. [16].

The results of our analysis are demonstrated in fig.3 where a solid line shows the dependence $\sigma_f(E)$ calculated for ^{215}At with $B_f = 15.3$ MeV. The barrier value we have obtained is in good agreement with the value $B_f = 15.5$ MeV obtained in the model of Myers and Swiatecki [18]. Other

approaches to the description of B_f [19,20] in the region of nuclei with $Z \cong 84$ produce results which are in agreement with [18], that is why it seems impossible to choose the most adequate model in this case.

It should be noted, that for the reaction studied $^{6}He + {}^{209}Bi$ the results of calculating $\sigma_f(E)$ depend strongly on the choice of parameters B_f and a_f / a_ν. That is why, even with the possible ambiguities in setting these data taken into account, the results of this analysis cannot serve as good enough grounds for the application of model [17] to the description of the input channel in reactions with ^{6}He.

3.3. Influence of Introduced Angular Momenta

In this subsection we are using, for a more spectacular representation of data, a different approach suggested in ref. [23] for separation of evaporation channels and compound nucleus fission. The cross section for evaporation of particles is written as follows:

$$\sigma_{evap}(E) = \sum_J \sigma_J(E) W(E^*, J), \tag{4}$$

where $W(E^*, J)$ is the survival probability for a nucleus in the evaporation cascade with passing by the fission channel.

For nuclei in the region $30 < Z^2/A < 35$ it has been found [23] that there exists for this value a sharp cut by the angular momentum

$$W(E^*, J) = \begin{cases} 1 & J < J_{evap} \\ 0 & J > J_{evap} \end{cases} \tag{5}$$

with the J_{evap} values independent of the input channel and the excitation energy of the compound nucleus. They are just linear functions of the parameter Z^2/A.

In this approximation the evaporation and fission cross sections can be written down in the following way:

$$\sigma_{evap}(E) = \frac{\pi}{k^2}(J_{evap} + 1)^2 \tag{6}$$

$$\sigma_{fiss}(E) = \pi R_b^2 (1 - V_b/E) - \frac{\pi}{k^2}(J_{evap} + 1)^2. \tag{7}$$

In the given expression for the sake of simplicity there has been used a classical expression for the fusion cross section in the near-barrier region, but in calculations we use a quasi-classical variant [24] of the single channel model of the critical distance [21]. At high energies of incident particle, where the contribution into the fusion cross section is made by many partial waves, the Coulomb barrier parameters in expression (7) are to be substituted by the parameters determining the potential at a distance $R_{cr} = A_1^{1/3} + A_2^{1/3}$ [21].

Thus, a strong dependence on the incident ion orbital angular momentum is contained both in the input and output channels. By parameterization of the potential from ref. [22] we have obtained for both the reactions the value of the potential at a critical distance $\cong -7$ MeV. The negative sign of the potential shows that at high energies of incident ions the fusion's full cross sections diminish with energy increase.

Having rewritten the fission cross section as:

$$\sigma_{fiss}(E) = \pi R_b^2 (1 - V_{eff}/E) \tag{8}$$

one can see that the fission cross section is well described by a known classical expression for the reaction cross section possessing though an «effective potential»:

$$V_{eff} = V_b + \frac{(J_{evap} + 1)^2 h^2}{2 \mu R_b^2}. \tag{9}$$

Based on this one can find the expression for the energy shift between the fusion cross section and the cross section of compound nucleus fission:

$$\Delta E = \frac{(J_{evap} + 1)^2 h^2}{2 \mu R_b^2}. \tag{10}$$

This formula points at a strong dependence of the energy shift on the reduced mass of the system, which in our case is 1.5 times greater for the reaction with ^{6}He than for the reaction with ^{4}He.

In the sharp cut approximation (5) one obtains a very steep slope in the fission cross sections at low energies that is why we have introduced an additional parameter ΔJ into the function W:

$$W(E^*, J) = \left[1 + \exp\left(\frac{J - J_{evap}}{\Delta J}\right)\right]^{-1}. \tag{11}$$

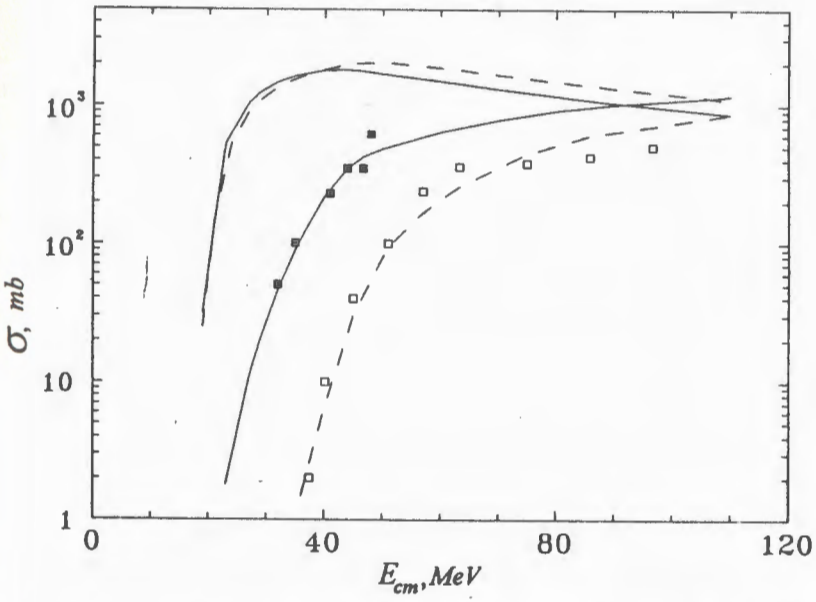

Fig.4. The result of calculating the dependence of fission and evaporation cross sections on the energy of bombarding particles (in the c.m.s.) ^{6}He (solid lines) and ^{4}He (dashed lines)

Parameters J_{evap} and ΔJ can be determined from the statistical theory of compound nucleus decay. In the given work we have calculated them as free parameters which were selected for better description of the data.

The results of calculating the evaporation and fission cross sections are presented in fig.4. The obtained parameters: $J_{evap} = 26.2$ and $\Delta J = 1.9$ for the reaction with ^{6}He and $J_{evap} = 26.2$ and $\Delta J = 0.9$ for the reaction with ^{4}He agree with the systematics [23] which gives for two reactions the J_{evap} values of $32\hbar$ and $29\hbar$, correspondingly.

We see that the threshold values of angular momenta at which there opens a fission channel are practically identical for both the reactions. Thus, the energy shift between the fission cross sections can be explained by different reduced masses in the input channels of these two reactions. To illustrate this statement we have presented in fig.5 the calculated partial cross sections of evaporation and fission in two reactions at an energy of 40 MeV in the center of mass system. One can see that in the reaction ^{6}He + ^{209}Bi a large angular momentum is introduced into the compound nucleus and the fission channel turns out to be open.

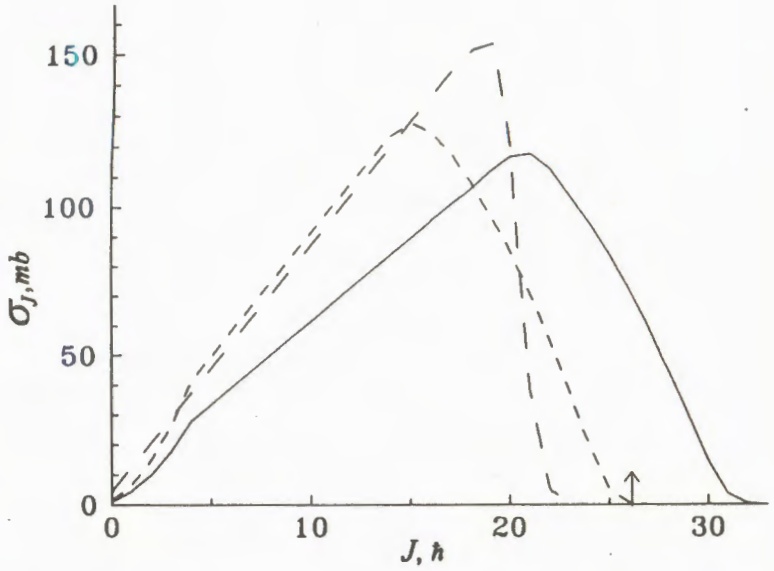

Fig.5. The calculated partial cross sections of fusion for the reaction ^{4}He + ^{209}Bi (short dashed lines) and ^{6}He + ^{209}Bi (solid lines) at an energy of 40 MeV (in the c.m.s.). The arrow points out the value of J_{evap}. Long dashed line denotes the calculation for ^{4}He disregarding the spin of ^{209}Bi nucleus

In the same figure one can find a calculation disregarding the spin of ^{209}Bi nucleus. It is evident that a large spin $9/2\hbar$ leads to the erosion of the upper limit of partial penetrations for fusion. In this case the dependence of the calculation results on parameters J and ΔJ appears to be very weak. Thus, the reaction of fusion with even-even nuclei are preferable for studying the competition of evaporation and fission.

Based on the factors considered above and on the experimental data available it is difficult to give preferences to either of them. The picture can be clarified through the comparison of the fission cross sections and of fission fragments angular distributions for two or three different input channels, leading to the same compound nucleus (for example in the reactions ^{6}He + ^{206}Pb and ^{4}He + ^{208}Pb or ^{6}He + ^{187}Os, ^{4}He + ^{189}Os and ^{187}Re + ^{6}Li). In this case $\sigma_{fiss}(E)$ and $W(\Theta)$ will mainly depend on the difference in the l_{cr} of the compared reactions or by the structure of the nucleus ^{6}He.

It is evident, also, that investigations on secondary beams open new possibilities for studying the fission of such compound nuclei, which are impossible to obtain in reactions with heavy ions at acceleration of stable isotopes.

In conclusion, the authors are pleased to express their gratitude for useful discussions to Yu.A.Muzychka, M.G.Itkis and for assistance in performing experiments on secondary beams — to the staff of the U400 accelerator, for invaluable assistance at constructing the rotating producing target — to G.N.Ivanov and V.B.Galinsky, for the transition into English — to V.I.Merzlyakov.

References

1. Tanihata I., Hamagaki H. et al. — Phys.Lett., 1985, B160, p.380.
2. Anne R., Arnell S.E. et al. — Phys.Lett., 1990, B250, p.19.
3. Lewitowicz M., Borcea C. et al. — Preprint CANIL, 1992, P-92-20; In: Proc. Inter. Conf. on Exotic Nuclei (Foros, Crimea, 1991), Ed. by Yu.E.Penionzhkevich and R.Kalpakchieva. World Scientific, Singapore, 1992, p.429.
4. Tanihata I. et al. — In: Proc. of 6th Conf. on Nuclei far from Stability (Bernkastel-Kues, July 1992, Germany) Ed. by R.Neugart and A.Wohr. Inst. Phys. Conf. ser, 1993 No.132, p.167.
5. Skobelev N.K., Lukyanov S.M., Penionzhkevich Yu.E. et al. — Z.Phys., 1992, A341, p.315.
6. Kolata J.J. et al. — Phys. Rev. Lett., 1992, 69, p.2631.
7. Ogloblin A.A. — In: Proc. Inter. Conf. on Exotic Nuclei, (Foros, Crimea, 1991), Ed. by Yu.E.Penionzhkevixh and E.Kalpalchieva. World Scientific, Singapore, 1992, p.36.
8. Zhukov M.V. et al. — Ibid. ref.7, p.84.
9. Lukyanov S.M. et al. — JINR Preprint, P7-91-224, Dubna, 1991, Lukyanov S.M. et al. — Ibid ref.7, p.415.
10. Abdulaev H. et al. — JINR Preprint, E12-3243, Dubna, 1967, Otgonsuren O. et al. — Atomic Energy (Russian), 1972, 33, p.979.
11. Ralarosy J. et al. — Phys. Rev., 1973, C8, p.2372.
12. Itkis M.G. — Particles and Nuclei (Russian), 1988, 19, p.701.
13. Alamanos N. et al. — Proc. Intern. Workshop on the Physics and Techniques of Secondary Nuclei Beams (March 23—25, 1992, Dourdan, France), Ed. by J.F.Bruandet. Frontieres. France, 1992, p.29.
14. Ericson T. — Adv. Phys., 1960, 9, p.425.
15. Ignatyuk A.V. et al. — Nuclear Physics (Russian), 1979, 21, p.1185.

16. Ignatyuk A.V. et al. — Particles and Nuclei (Russian), 1985, 16, p.709.
17. Bass R. — Phys. Lett., 1973, B3, p.47; Nucl. Phys., 1974, A231, p.45.
18. Myers W.D., Swiatecki W.J. — Ark.Fys., 1967, 36, p.343.
19. Myers W.D. — Droplet Model of Atomic Nuclei, IFI/Plenum N.Y., 1977.
20. Krappe H.J. et al. — Phys.Rev., 1979, B20, p.992.
21. Glas D., Mosel U. — Phys.Rev., 1974, C10, p.2620.
22. Broglia R.A., Winter A. — In: Heavy Ion Reactions, Benjamin/Cummings. Merlo Park, CA, 1981, v.1, p.114.
23. Matsuse T. — Proc. of the Tsukuba Int. Symp., Ed. by K.Furuno, T.Kishimoto, Singapore 1984, p.113.
24. Tarakanov A.V. et al. — Nuclear Physics (Russian), 1991, 53, p.1285.

Received on July 9, 1993.

УДК 539.1.074.3+539.1.074.6

A LARGE AREA CsI(Tl) DETECTOR FOR THE SCINTILLATOR SHELL OF FOBOS*

W.Wagner[1], A.S.Fomichev, H.-G.Ortlepp[1], C.-M.Herbach[1], A.Matthies[1], G.Pausch[2], O.V.Strekalowskij, M.A.Milovidov[3], V.A.Vitenko[3]

A large area CsI(Tl) detector for the 4π-array FOBOS has been investigated. The response nonuniformity was reduced to 5% by use of a hollow light guide. The energy resolution amounts to 6—7% for 5 MeV alpha particles.

The investigation has been performed at the Flerov Laboratory of Nuclear Reactions, JINR.

Большой CsI(Tl) детектор для сцинтилляционной части установки ФОБОС

В.Вагнер и др.

Исследовался CsI(Tl) детектор большой площади для 4π-установки ФОБОС. Неравномерность отклика была уменьшена до 5% с использованием пустотельного световода. Полученное энергетическое разрешение для альфа-частиц энергии 5 МэВ составляет 6—7 %.

Работа выполнена в Лаборатории ядерных реакций им.Г.Н.Флерова ОИЯИ.

The 4π-multidetector-array FOBOS [1] coming into operation this year in the Flerov Laboratory of Nuclear Reactions at JINR Dubna consists of an inner gas detector array and an outer scintillator shell to register intermediate and heavy fragments produced in heavy ion induced nuclear reactions as well as more penetrating light charged particles (LCP).

The large area CsI(Tl) detector presented here (fig.1) is one element of the scintillator shell of altogether 210 hexagonal crystals (enveloping circles with ∅ = 200 mm and ∅ = 150 mm) arranged in mosaiclike modules of at

*This work is part of the FOBOS project financially supported by the BMFT, Bonn, Germany under Contract No.06 DR 100

[1]at present JINR Dubna; on leave from Research Center Rossendorf Inc., Dresden, Germany

[2]Freie Universität Berlin, Germany

[3]V.G.Khlopin Radium Institute, St.Petersburg, Russia

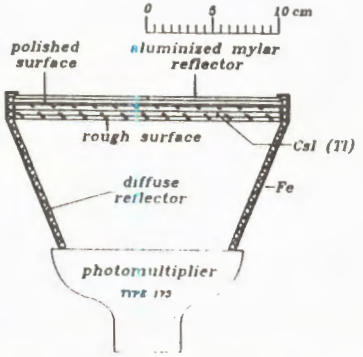

Fig.1. Schematic view of the large area CsI(Tl) detector

that time 7 hexagons which are situated behind the 30 Bragg ionization chambers covering them with 73.4% geometrical efficiency. Crystal thicknesses of 10 mm and 15 mm were chosen for angles of $\vartheta = 53°—164°$ and $\vartheta = 16°—52°$ to stop LCP with energies of up to 50 and 65 AMeV, respectively. Applying pulse-shape discrimination (PSD) [2] LCP can be well separated in relation to mass and charge for $Z \leq 4$ [3,4].

This is demonstarted in fig.2, where we used the reaction ^{20}Ne (9.1 AMeV) + ^{58}Ni and the large CsI(Tl) detector was situated at $\vartheta = 45°$ relative to the beam axis at a distance of 70 cm from the target [5]. The main problem of using large scintillators is the reduction of the position dependent detector responce induced by

(i) the nonuniform light output of the crystal,

(ii) the nonuniform photocathode sensitivity and photoelectron collection efficiency of the photomultiplier (PM),

(iii) the position dependent light collection effiiciency.

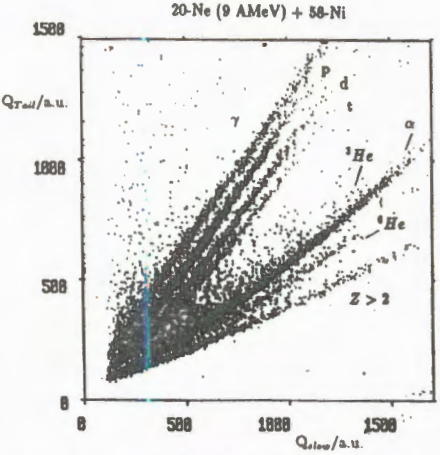

Fig.2. Pulse-shape discrimination of LCP with the large area CsI(Tl) detector integrating the current pulses of the PM within time gates of $\Delta t_1 = 0—400$ ns (Q_{slow}) and $\Delta t_2 = 1600—3600$ ns (Q_{tail})

The crystals delivered by MONOCRYSTALREACTIV, Kharkov, Ukrain, were grown under vacuum applying Kyropoulos' method. The content of Tl activator amounts to 0.07—0.08% which is an empirical optimum for high light output as well as good PSD properties for LCP. The samples were cut from the central part of the $\varnothing = 500$ mm ingots and polished using organic solvents to avoid a dead layer at the surface.

Scanning the crystals with the help of an alpha source and a small diameter phototube, the radial nonuniformity of light output ΔL induced by an inhomogeneous

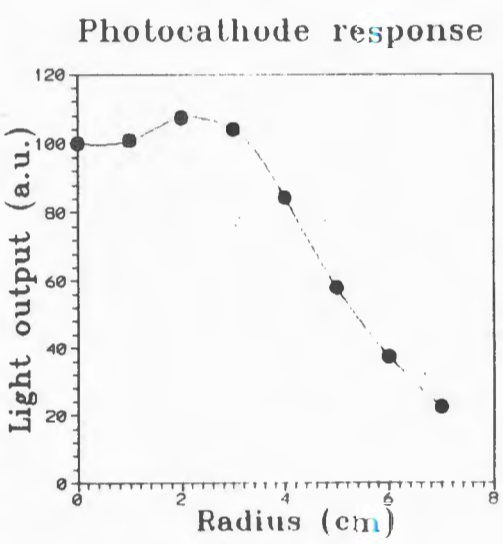

Fig.3. The radial photocathode responce of PM FEU 173 measured with a small (∅ = 10 mm) CsI(Tl) crystal directly coupled to the PM and a ^{137}Cs source

dopant concentration was checked to be less than 2%.

The scintillation light has to be matched to the PM in such a manner that the nonuniform photocathode response (see fig.3) is averaged, a maximum light collection and a minimum dependence on the position of the light source within the crystal volume is achieved. We coupled the crystal to a spectroscopic PM of type FEU 173 (EKRAN, Novosibirsk, Russia) which has a large (∅ = 150 mm) trialcali photocathode with high

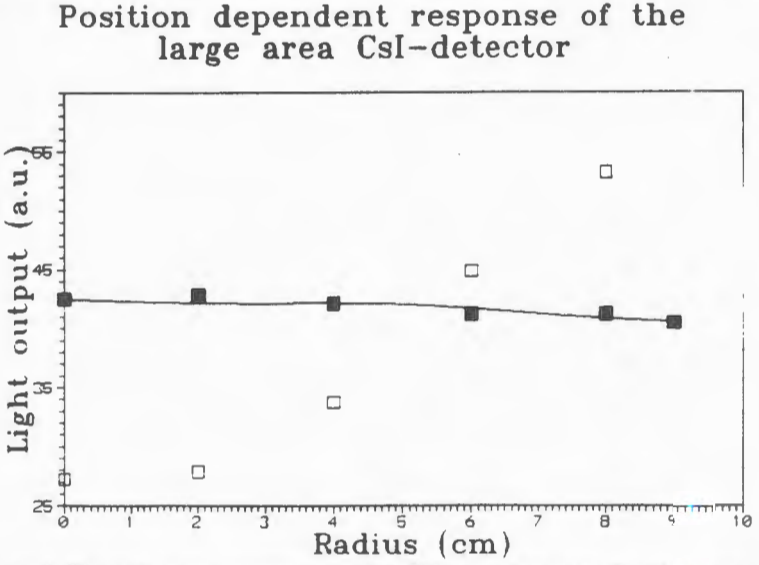

Fig.4. The light output measured for a ∅ = 200 mm, 15 mm thick CsI(Tl) crystal coupled by a plexiglas light guide to PM FEU 173 (open squares) and coupled by a hollow diffuse reflecting light guide to PM FEU 173 (full squares) in dependence on the radial position of the alpha source. The line represents a simulation of the light collection for a hollow light guide (K = 0.9) normalized to the data at the centre of the crystal

photochatode sensitivity of typical $(1.5— —2.5)\cdot 10^{-4}$ A/lm and due to its spectral sensitivity range of $\lambda = 300—850$ nm is ideally adapted to the emission spectrum of CsI(Tl) ($\lambda_{max} \approx 550$ nm).

Monte-Carlo-simulations of light transport from the crystal to the PM were carried out for several types of light guides considering light absorption and reflection from different surfaces. As it is shown in fig.4 the coupling by e.g. a conventional plexiglas light quide leads to a very large radial variation of light collection up to a factor of two.

In our conditions a conical shaped hollow light guide with a diffuse reflecting inner surface ($h = 110$ mm, $\varnothing = 150$ mm at the PM) was found to be the best solution. It is made from zinc plated sheet metal painted with white TiO_2 enamel and parallelly serves as crystal support allowing a trivial design of the CsI(Tl) mosaics of the scintillator shell.

In the case of a hollow light guide it was found that the read-out of scintillation light from the crystal is enhanced if its back side is optically rough to avoid total inner reflection at the read-out surface and subsequently absorption losses of light. The light output was measured to be nearly 30% higher compared with polished crystals.

Results of simulations as well as experimental data obtained with an alpha source are given in the table and fig.4. The remaining radial variation of the light output amounts to 5%. The measurement well agrees with the simulation for an assumed reflectivity of the light guide surface of $K \approx 0.9$ what seems to us to be a realistic value for the enamel used. Indeed the value of the reflectivity K is the critical parameter determining the remaining ΔL (see tab.).

Due to the rough read-out surface of the crystal and the diffuse reflecting surface of the hollow ligh quide the radial nonuniformity of the photocathode response of the PM FEU 173 (fig.3) will be well averaged due to the nearly homogeneous illumination and, therefore, its influence on energy resolution is minimized.

Table

K	R (cm)					ΔL (%)
	0.00	2.47	4.95	7.42	9.90	
0.99	52.7	52.7	52.7	52.5	52.4	0.6
0.90	42.5	42.1	42.0	41.0	40.5	4.8
0.80	34.1	33.6	33.0	32.2	31.7	7.3
060	24.2	23.5	23.0	22.1	21.0	14.1

In summary we obtained an energy resolution of 6—7% for collimated alpha particles and typically 9% if the ^{238}Pu alpha source was positioned at a distance of 50 cm from the front side simultaneously illuminating the whole crystal.

References

1. Ortlepp H.-G. et al. — Proc. Int. Conf. on New Nuclear Physics with Advanced Techniques, Ierapetra, Crete, Greece (1991) and Proc. Int. School Seminar on Heavy Ion Physics, Dubna, (1993).
2. Alarja J. et al. — Nucl. Instr. and Meth., 1986, A242, p.352.
3. Stracener D.W. et al. — Nucl. Instr. and Meth., 1990, A294, p.485.
4. Drain D. et al. — Nucl. Instr. and Meth., 1989, A281, p.528.
5. Fomichev A.S. et al. — JINR P15-92-50, Dubna, 1992.

Received on August 18, 1993.

УДК 539.172.17

HOT FUSION REACTION CROSS-SECTIONS

Yu.A.Muzychka, B.I.Pustylnik

In the frame of the statistical theory of decay of compound nuclei we suggested a simple parametrization which allows for satisfactory reproduction of the complete set of experimental data on the cross-sections of (HI, xn) reactions for the bombarding ions lighter than $A < 40$ and for compound nuclei with $Z > 100$. We came to an observation that the value of the xn-reaction cross-section depends, besides the Γ_n / Γ_f ratios for each step of the evaporation cascade, also oh the value of the «survival zone» that is determined completely by the fission barrier. The cross-sections of $4n$- and $5n$-reactions are calculated for a number of projectile-target combinations leading to the formation of evaporation residues in the region of heavy transfermium nuclides.

The investigation has been performed at the Flerov Laboratory of Nuclear Reactions, JINR.

Сечение реакций горячего слияния

Ю.А.Музычка, Б.И.Пустыльник

В рамках статистической теории распада составных ядер предложена простая параметризация, позволившая получить хорошее описание всей совокупности имеющихся экспериментальных данных о сечениях (HI,xn)-реакций, вызываемых ионами легче аргона, для составных ядер с $Z > 100$. Показано, что величина сечения для xn-реакцнй в этой области ядер определяется не только отношениями испарительной и делительной ширин Γ_n / Γ_f для каждой ступенн испарительного каскада, но и величиной «зоны выживаемости» в конце испарительного каскада, напрямую связанной с величиной барьера деления. Сделаны расчеты сечений $4n$- и $5n$-реакций для ряда комбинаций ион-мишень, приводящих к образованию изотопов тяжелых трансфермиевых элементов.

Работа выполнена в Лаборатории ядерных реакций им.Г.Н.Флерова ОИЯИ.

During recent years, the interest to «hot» fusion reactions, using actinide targets, in which compound nuclei with excitation energy of 40-50 MeV are produced, has increased [1]. At present there is a great amount of experimental data on cross-sections of such reactions with evaporation of 4-6 neutrons leading to different isotopes of the transfermium elements up to the element 106, that allows one to carry out a systematic analysis of these data.

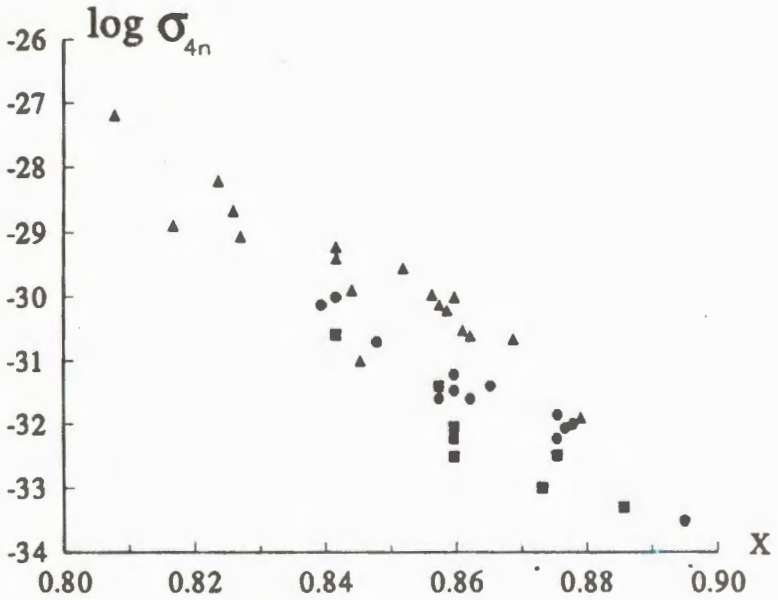

Fig.1

Figure 1 shows the values of cross-section logarithms in the maxima of excitation functions of 4n-reactions versus X — the fissility parameter of the original compound nucleus. Triangles are the values of σ_{4n}^{max} for reactions induced by B and C ions, circles — N, O, F, squares — Ne, Mg, Al. The «quiet», without any peculiarities behaviour of σ_{4n}^{max} is noteworthy. All points are sufficiently uniformly grouped around one straight line which implies an exponential dependence of σ_{4n}^{max} on X. A similar picture is observed for $5n$-reaction cross-sections (Fig.2). It is seen that for the nuclei under consideration no substantial changes occur in the xn-reaction process and all experimental data can be described using a unified algorithm. Usually one uses relations of the statistical theory of nuclear reactions for this purpose, but there exist some doubts in their validity for the fission width calculations when the fission barrier and nucleus temperature are approximately equal. At the same time, the data on the precission neutrons number obtained during the recent years indicate that fission is a slow process. This circumstance and also the exponential dependence of xn-reaction cross-sections leading to transfermium nuclei on the fissility parameter X indicate that one can try to use formalism of the statistical

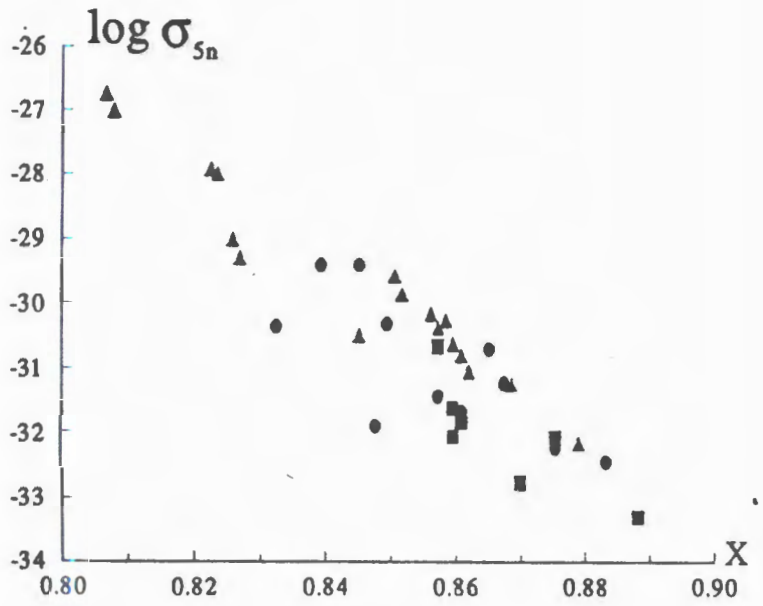

Fig.2

theory of nuclear reactions. In our calculations a statistical code based on the program ALICE was employed [2]. The cross-section of the compound nucleus formation was calculated using the formula:

$$\sigma_c = \frac{\pi}{k^2} \sum_{l=0}^{l_\sigma} \frac{2l+1}{1+\exp(2\pi\,(V_B(l) - E_{cm}) \,/\, \hbar\,\omega_l)}, \qquad (1)$$

where $V_B(l)$ is the height of the interaction barrier and ω_l is the curvature of this barrier. The choice of parameters of the interaction potential was discussed earlier [2]. The aim of our calculations was the optimum description of the maximum values of cross-sections. More than 90% of cross-section values in their maxima are achieved at $l \ll l_{cr}$. For this reason, the results of calculations were not much sensitive to the value of l_{cr} and calculations were ended when contribution of the last partial wave to the cross-section was less than 1% of its value.

Calculations were carried out in two variants. In the first one, shell effects in evaporation and fission channels were taken into account:

$$a(E) = a\{1+[1-\exp(-0.0054E)]\Delta W/E\} \quad B_f(l) = B_f^{\mathrm{CPS}}(l)+\Delta B, \quad (2)$$

where $a = A/10$, ΔW and ΔB are the shell corrections to the masses of the residual nucleus after neutron evaporation and of the fissioning nucleus, $B_f^{CPS}(l)$ is the fission barrier in the model of rotating charged drop. The ratio a_f / a_n was taken equal to 1.

In the second case the relations (2) were used also, but the values ΔW and ΔB were considered to be formal parameters. For their determination the reaction $^{248}U+^{18}O$ was used, for which excitation functions of the reactions from $4n$ to $8n$ were measured with a good accuracy. The best fit was obtained with $\Delta W = 0$ and $\Delta B = 1.1$. These values of parameters were fixed and calculations for all reactions, for which experimental data exist, were performed with them. In both variants of calculation a good fit was obtained. We consider the second variant which is more simple and more convenient for extrapolation. The results are presented in Fig.3, where there is shown a logarithm of the ratios of calculated and experimental values of cross-sections in maxima of excitation functions for reactions $4n$, $5n$ and $6n$ versus fissility parameter X. Dashed lines limit interval $-0.6 < \log(\sigma_{cal}/\sigma_{exp}) < 0.6$, i.e., for the points lying between these lines $1/4 < \sigma_{cal}/\sigma_{exp} < 4$. From Fig.3 one can see that overwhelming majority of the points are within this interval.

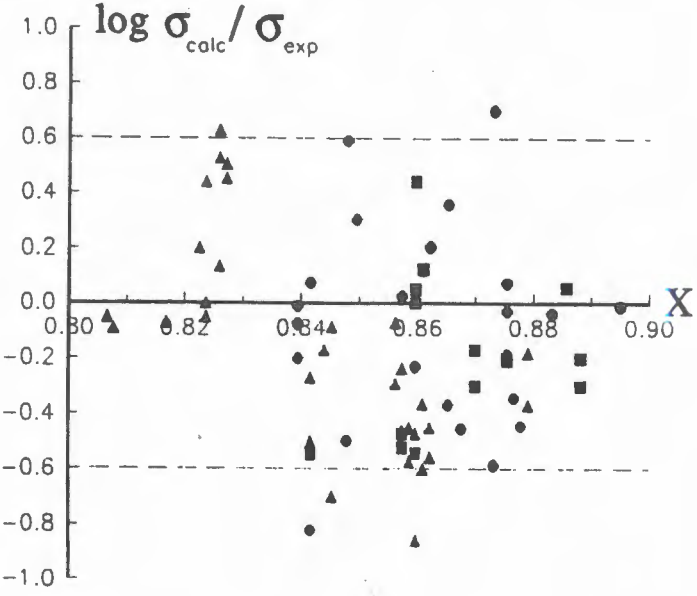

Fig.3

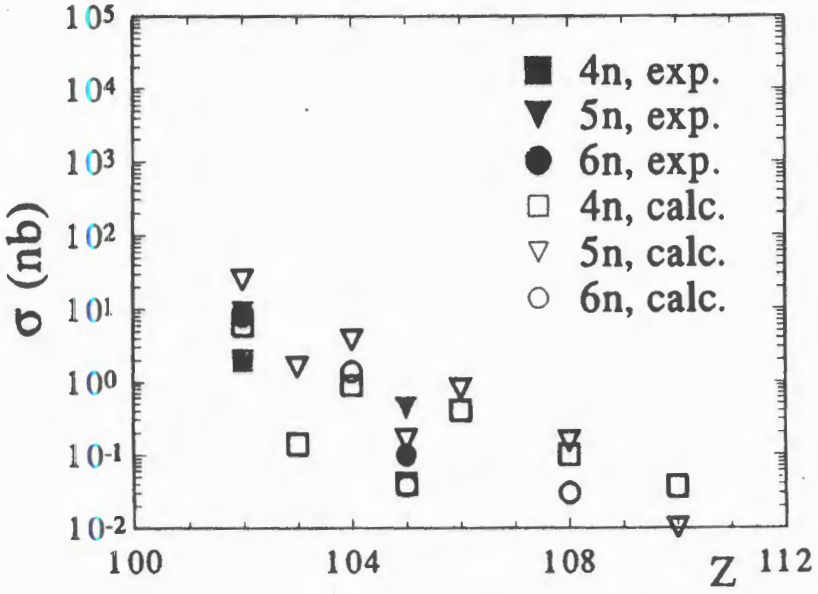

Fig. 4

One must note that the fission barriers of transfermium nuclei B_f are substantially smaller than their neutron binding energies and therefore after neutron cascade a nucleus can be found with high probability with an excitation energy within interval $B_n - B_f$ and it undergoes fission. Only those nuclei reliably survive that after neutron cascade have the excitation energy smaller than B_f. Calculations show that this factor reduces yield of heavy nuclei by several orders of magnitude and that the value of $\langle \Gamma_n / \Gamma_f \rangle$ ratio is smoothly varying in the transfermium region and ranges near 0.1. This result qualitatively differs from the generally accepted opinion that the ratio σ_{xn}/σ_c is completely determined by $\langle \Gamma_n / \Gamma_f \rangle$ value which for heavy nuclei is of the order of 0.01.

A good agreement of calculation results and experimental data for reactions induced by Mg and Al, in which isotopes of the elements 102 and 105 were produced, is exemplified by Fig.4. This agreement indicates that there are no sensible limitations in fusion for this ions. Some estimates of production cross-sections of several isotopes of the elements 107—110 in maxima of excitation functions for $4n$-and $5n$-channels are listed in the table.

Table

Reaction	E_l (MeV)	$4n$ E^* (MeV)	σ (pb)
$^{243}Am+^{26}Mg$	138	42.9	110
$^{249}Cf+^{22}Ne$	118	41.2	120
$^{248}Cm+^{26}Mg$	138	42.4	110
$^{248}Cm+^{27}Al$	150	46.9	10
$^{242}Pu+^{36}S$	187	41.2	90
$^{242}Pu+^{34}S$	185	44.5	14
$^{249}Cf+^{26}Mg$	144	42.3	37

Reaction	E_l (MeV)	$5n$ E^* (MeV)	σ (pb)
$^{243}Am+^{26}Mg$	146	50.1	89
$^{249}Cf+^{22}Ne$	128	50.4	58
$^{248}Cm+^{26}Mg$	146	49.6	150
$^{248}Cm+^{27}Al$	154	50.5	33
$^{242}Pu+^{36}S$	196	49.0	25
$^{242}Pu+^{34}S$	193	51.5	10
$^{249}Cf+^{26}Mg$	154	51.3	10

References

1. Flerov G.N., Ter-Akopian G.M. — Prog. Part. Nucl. Sci., 1987, v.19, p.197.
2. Muzychka Yu.A., Pustylnik B.I. — In: Proc. Int. School-Seminar on HI Phys., Dubna, 1983, JINR D7-83-644, Dubna, 1983, p.420.

Received on July 22, 1993.

УДК 546.751.78

CHEMICAL IDENTIFICATION OF ELEMENT 106 BY THERMOCHROMATOGRAPHIC METHOD

S.N.Timokhin, A.B.Yakushev, Xu Honggui,
V.P.Perelygin, I.Zvara

For the first time the chemical identification of element 106 has been accomplished. Im comparative gas thermochromatographic studies of (oxo)chlorides of element 106 and of tungsten, reproducible groups of tracks of fission fragments from s.f. of $^{263}106$ were observed in a temperature region of 150—250 °C. This provides evidence that the element 106 oxochloride is similar to the tungsten compound. Elements 104, 105 and actinoids do not yield volatile compounds under the particular experimental conditions.

The investigation has been performed at the Flerov Laboratory of Nuclear Reactions, JINR.

Химическая идентификация элемента 106 термохроматографическим методом

С.Н.Тимохин и др.

Впервые была выполнена химическая идентификация элемента 106. В сравнительных термохроматографических экспериментах с (окси)хлоридами элемента 106 и вольфрама наблюдали воспроизводимые зоны треков осколков спонтанного деления элемента 106 в интервале температур 150—250 °С. Это служит доказательством тому, что оксихлорид элемента 106 подобен аналогичному соединению вольфрама. Элементы 104, 105 и актиноиды не дают летучих соединений при данных экспериментальных условиях.

Работа выполнена в Лаборатории ядерных реакций им.Г.Н.Флерова ОИЯИ.

As an expected transition metal of group VI of the Periodic System, element 106 must form volatile chloride(s) and oxochloride(s). In experiments with isotopes of tungsten [1] we found a chemical system for selective separation of an oxochloride of W from Ln, Hf and Ta, which would serve the title goal.

Element 106 was produced at the U-400 cyclotron through the reaction

$$^{18}O(94\ MeV) + {}^{249}Cf = {}^{263}106 = 4n.$$

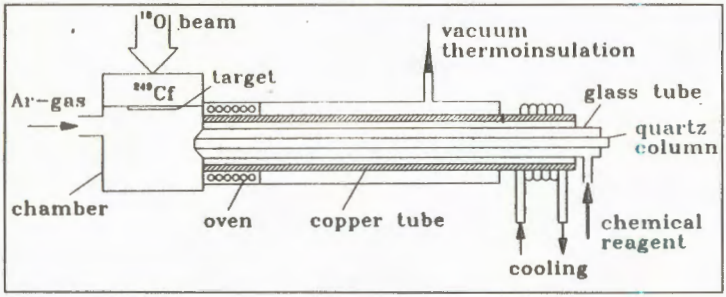

Fig.1

For ^{263}106 a cross section of 0.4 at 94 MeV for the s.f. branch and $T_{1/2}$ of 0.9 s were reported [2]. The target contained 1.0 mg/cm^2 of radiochemically very pure ^{249}Cf. The ^{18}O beam intensity was about $3 \cdot 10^{12}$ pps. A schematic of our gas chromatographic equipment is shown in Fig.1.

The thermalized reciols were injected into a quartz thermochromatographic column with 1 l/min argon gas. As chemical reagents we used air (0.2 l/min) saturated with $SOCl_2$ (20 mmHg) vapors. The nuclide ^{263}106 was registered through its s.f. events — the surface of the column itself served as the track detector of fission fragments.

In two experiments we put a quartz wool filter in the start zone (Fig.1, oven). No fission fragment tracks were found in the column. In subsequent two experiments such a filter was absent. This time, reproducible zones of tracks of fission fragments were observed in a temperature region of 150—250 °C (Fig.2), close to the deposition temperature of the 16-s $^{166}W^{-1}$ [1]. Then s.f. events during a 20-h bombardment and nineteen events in a 32-h one were registered in this region; in 3 and 6 cases, respectively, both fission fragments from an event were detected (see «black» events in Fig.2).

Essentially no tracks were found in the start zone and outside the indicated region of the thermal gradient. At the same time, various α-active actinoid isotopes ($^{252-254}$Fm, ^{253,254}Es, ^{248}Cf) produced in the «transfer» reactions were seen mostly in the start zone ($\cong$ 99%), i.e. the 106/An separation was as required.

The yields of ^{252}Fm, ^{256}Fm and ^{256}Md and recoiling from the particular target versus energy were measured for 91 to 104 MeV ^{18}O ions using catcher foils and direct counting of relatively long α-active and s.f. nuclides. The results are summarized in the Table. Our yields for the ^{252,256}Fm drop

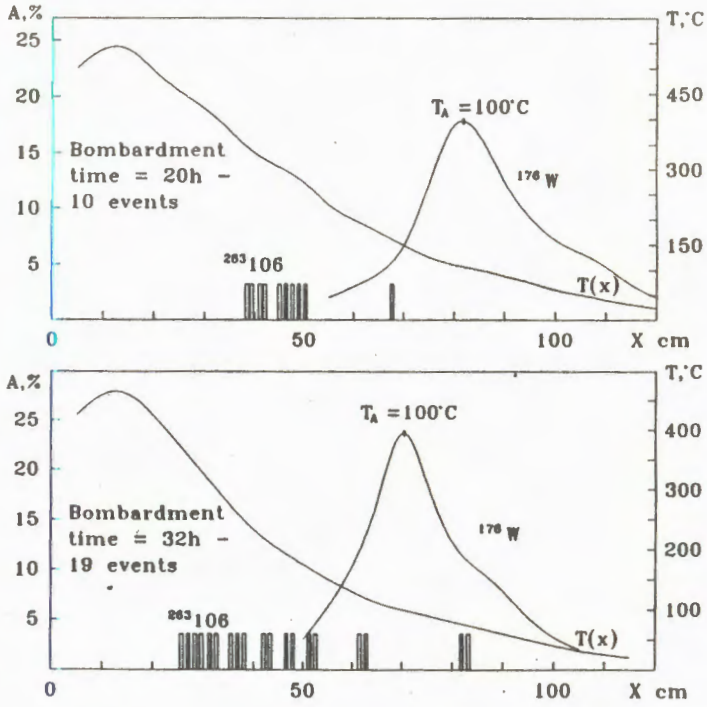

Fig.2

Table. Production cross sections for ^{252,256}Fm and ^{256}Md (in μb)

		91 MeV	94 MeV	97 MeV	104 MeV
Lee (LBL):	^{252}Fm	610	—	1910	2400
	^{256}Fm	0.11	—	1.2	1.5
	^{256}Md	0.07	—	0.69	0.19
Sagaidak (FLNR):	^{256}Fm	—	0.002	0.02	0.02
	^{256}Md	—	0.02	0.2	0.2
This work (FLNR):	^{256}Fm + ^{256}Md	10^{-4}	10^{-4}	0.02	0.02
	^{252}Fm	$2\cdot10^{-4}$	0.7 ± 0.3	43 ± 4	36 ± 4

sharply with the energy decreasing from 97 to 91 MeV. In the Table, the cross sections from D.Lee et al. [3] and R.Sagaidak et al. [4] are also given. The results of various authors in the Table cannot be directly compared

because the transfer reaction products have broad angular and projected range distributions, hence the recoil yield depends on the thickness of the target, which was not the same in the cited studies. The data need a separate evaluation.

We also made two 3-h bombardments at 94 MeV, in which the reaction products were carried by inert gas and deposited in a cold column. No fission events were detected in the column: i.e., the total yield of «background» s.f. activities with $Z < 106$ and half-lives longer than some 0.1 s does not exceed the yield of element 106.

Our data seem to confirm the formation of an element 106 oxochloride similar in properties to the tungsten compound. One should bear in mind ^{176}W that has a half-life of 2.5 h, and due to this it is deposited at much lower temperature than a 0.9 s tungsten activity would be. Unfortunately there is no way to produce ^{166}W or even shorter tungsten isotopes simultaneously with element 106.

In the first two «unsuccessful» experiments, obviosly, the retention time on the filter exceeded $T_{1/2}$ of $^{263}106$. Longer retention on filters was observed earlier also for elements of groups IV and V.

Thus, for the first time the chemical identification of element 106 was accomplished. Both the experiments with Hf and Ta and our earlier studies of elements 104 and 105 in very similar chemical systems exclude the possibility that the latter two transactinoid elements might be responsible for the observed fission events.

References

1. Yakushev A.B. et al. — In: Heavy Ion Physics, JINR-FLNR Scientific Report 1991—1992. JINR E7-93-57, Dubna, 1993, p.169.
2. Druin V.A. et al. — JINR Commun., P-12056, Dubna, 1978.
3. Lee D. et al. — Phys. Rev., 1983, 27, p.6.
4. Sagaidak R.N. et al. — JINR Commun., P7-82-890, Dubna, 1982.

Received on October 7, 1993.

УДК 539.1.074.4

DIFFRACTIONLIKE EFFECTS IN ANGULAR DISTRIBUTION OF CHERENKOV RADIATION FROM HEAVY IONS

E.S.Kuzmin, A.V.Tarasov

Formulae have been obtained for calculating the angular density of Cherenkov radiation from heavy ions with allowance for slowing-down of particle in the radiator. The diffraction structure of the angular spectrum of Cherenkov radiation (Fresnel diffraction) with the diffraction parameter dependent on the energy loss rates of particles is predicted.

The investigation has been performed at the Laboratory of Nuclear Problems, JINR.

Дифракционноподобные эффекты в угловом распределении черенковского излучения тяжелых ионов

Е.С.Кузьмин, А.В.Тарасов

Получены формулы для расчета угловой плотности черенковского излучения тяжелых ионов с учетом торможения частиц в радиаторе. Предсказан эффект дифракционной структуры углового распределения черенковского излучения (дифракция Френеля) с параметром дифракции, зависящим от удельных потерь энергии.

Работа выполнена в Лаборатории ядерных проблем ОИЯИ.

Tamm — Frank's theory [1] describes Cherenkov radiation of a particle that moves steadily and rectilinearly in a medium with the refractive index $n > c/v$ (v is the particle velocity, c is the speed of light in vacuum). So, this theory ignores interaction between the particle and the radiator material, while this interaction results in particle trajectory bending (multiple scattering) and in systematically decreasing velocity (ionization losses).

Dedrick [2] was the first to take into account the influence of the particle-radiator interaction on the angular density of the particle's Cherenkov radiation. He examined the influence of multiple scattering, while ignoring the slowing-down effect.

Below we consider another limiting case where the multiple scattering effect is insignificant, and it is the slowing-down effect that plays a leading part in forming the angular distribution of Cherenkov radiation. It occurs when nuclei of heavy elements (Z, $A \gg 1$) transverse thin radiators.

Ignoring fluctuations of energy losses, we shall assume that at each moment of time the particle has a very definite energy and thus a very definite velocity. Since we ignore the trajectory bending effect as well, our task is reduced to examining the angular distribution of the Cherenkov radiation emitted by a particle moving rectilinearly at a varying velocity. The answer can be found from the formulae of classical electrodynamics

$$\frac{dW}{d\omega\, d(\cos\theta)} = \frac{(ze\sin\theta)^2}{2\pi c^2} k\omega \left\{\int_0^L \exp[i\,\Phi(x)]dx\right\}^2, \qquad (1)$$

$$\Phi(x) = kx\cos\theta - \omega t(x); \quad t(x) = \int_0^x \frac{dx'}{v(x')}.$$

Here $dW/d\,\omega d(\cos\theta)$ is the spectral angular distribution of the radiation; k, ω are the wave number ($k = \omega\, n/c$) and the frequency of the Cherenkov photon; L is the thickness of the radiator; n is its refractive index, θ is emitting angle; ze is the ion charge.

Taking for thin layers of the radiator

$$\frac{1}{v(x)} \approx \frac{1}{v_0} - \frac{1}{v_0^2} v_0' x; \quad v_0' = \left.\frac{dv(x)}{dx}\right|_{x=0} < 0,$$

$$\frac{dv}{dx} = \frac{dE}{dx}\frac{dv}{dE} = \frac{1}{P}\left(1 - \frac{v^2}{c^2}\right)\frac{dE}{dx}; \quad P = Ev,$$

where $v_0 = v(0)$ is the particle velocity on entering the radiator; P, E are the momentum and the energy of the particle, we finally get

$$\frac{dW}{d\,\omega d(\cos\theta)} = \omega L\left(\frac{ze\sin\theta}{c}\right)^2 \cdot f(\theta, \omega),$$

$$f(\theta, \omega) = \frac{1}{2\Delta\theta\sin\theta_0} \cdot \{[C(u_1) - C(u_0)]^2 + [S(u_1) - S(u_0)]^2\}, \qquad (2)$$

where

$$C(u) = \sqrt{\frac{2}{\pi}} \int_0^u \cos t^2 dt, \quad S(u) = \sqrt{\frac{2}{\pi}} \int_0^u \sin t^2 dt -$$

are Fresnel integrals, and

$$u_{0,1} = \frac{n \cos\theta - \omega/v_{0,1}}{a}; \quad a = \sqrt{-\frac{2\omega v_c'}{v_0^2}},$$

$$\theta_{0,1} = \arccos\frac{c}{nv_{0,1}}; \quad \frac{1}{v_1} = \frac{1}{v_0} - \frac{1}{v_0^2} v_1' L; \quad \Delta\theta = \theta_0 - \theta_1 \approx \frac{|v_0'|L}{v_0} \cot\theta_0,$$

$$\int_{-1}^{1} f(\theta, \omega) d\cos\theta = 1,$$

Here v_1 is the particle velocity on leaving the radiator. The radiator thickness being small, Cherenkov radiation is concentrated in a narrow angular interval $\theta_1 \le \theta \le \theta_0$, $(\theta_0 - \theta_1 << 1)$. Within this interval and in the close proximity to it variables $u_{0,1}$ can be expressed as

$$u_{0,1} = \frac{\tan\theta_{0,1}(\theta - \theta_{0,1})}{\theta_d}; \quad \theta_d^2 = \frac{|v_0'|\lambda}{\pi c},$$

where λ is the radiation wave length.

As an example, we give a distribution for the angular density of Cherenkov radiation as it follows from the Tamm — Frank theory [1]

$$f_{T-F}(\theta, \omega) = \frac{1}{\delta\theta}\left(\frac{\sin x}{x}\right)^2; \quad x = \frac{\pi}{\delta\theta}\left(\cos\theta - \frac{c}{v_0 n}\right). \qquad (3)$$

The Tamm — Frank distribution width is defined as $\delta\theta = \lambda/nL$, where $\lambda = 2\pi c/\omega$ — is the radiation wave length.

In our opinion, distributions (2) and (3) essentially differ in the following features (see figs.1a, 1b).

As compared with distribution (3), the centre of gravity in distribution (2) is shifted toward smaller angles by $\Delta\theta/2$. The width of (2) is much larger than that of the Tamm — Frank distribution, and it increases proportionally with the radiator thickness. The opposite situation is typical of distribution (3), whose width decreases in inverse proportion to the ratiator thickness.

Speaking in terms of optics, we may compare the angular density of Cherenkov radiation from a steadily decelerating particle to the Fresnel slot diffraction, while radiation from a steadily moving particle is distributed in accordance with the Fraunhofer diffraction pattern. Moreover, if in the

Tamm — Frank theory the distance between maxima (the diffraction parameter) is determined by the wave length and the radiator thickness, $\delta\theta = \lambda/nL$ in distribution (2), the expression for the diffraction parameter involves energy loss rates in the radiator material

$$\theta_d^2 = \frac{|\nu_0'|\lambda}{\pi c} = \frac{1}{\pi\beta_0}(1-\beta_0^2)\left|\frac{dE}{dx}\right|\frac{\lambda}{E_0}, \quad \beta_0 = \frac{\nu_0}{c}.$$

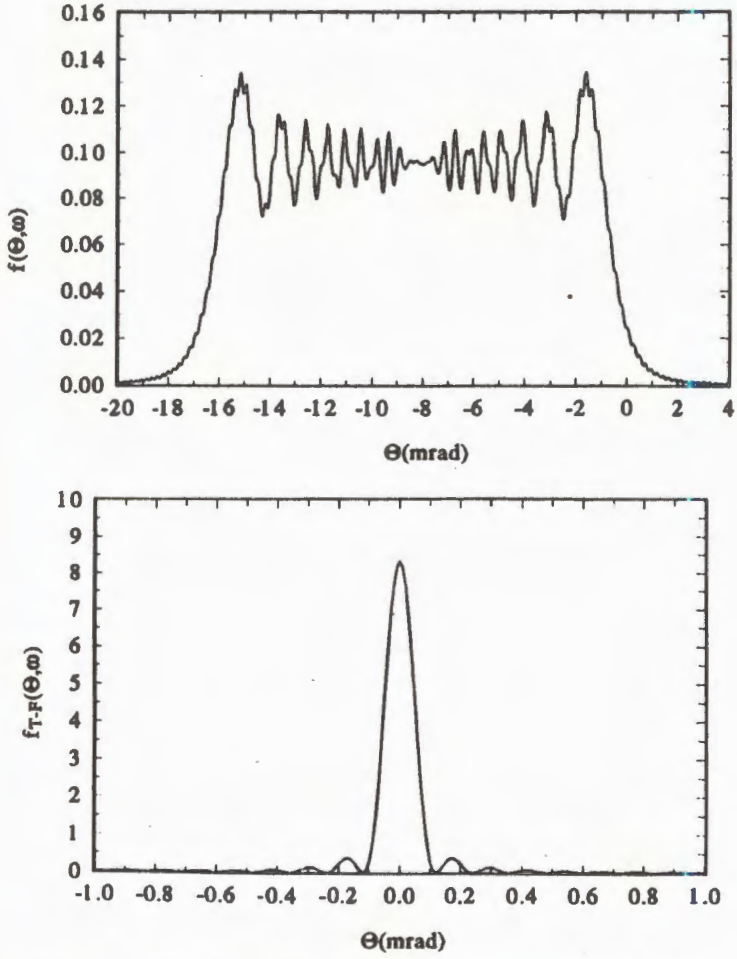

Fig.1. Distributions (2) and (3) calculated for gold nuclei of energy 1000 MeV per nucleon incident on a quartz radiator 0.5 cm thick. a) this paper; b) Tamm — Frank distribution

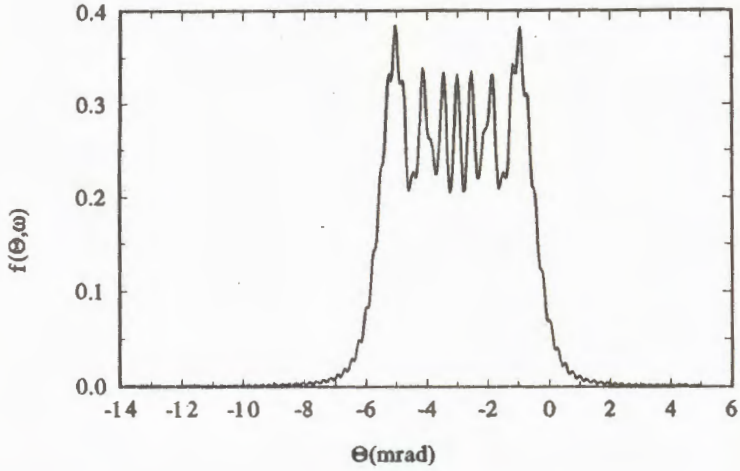

Fig.2. Distributions (2) calculated for iron nuclei of energy 1000 MeV per nucleon incident on a quartz radiator 0.5 cm thick

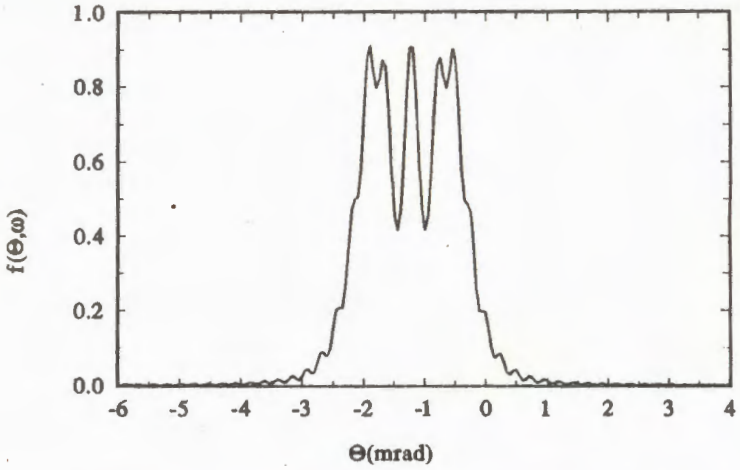

Fig.3. The same as in fig.2 but for neon nuclei of energy 1000 MeV per nucleon

The most distinct Fresnel-like diffraction pattern shows up in Cherenkov radiation of very heavy ions (uranium, gold), though its manifestations are observed with lighter nuclei as well.

In figs.2,3 there are angular distributions of Cherenkov photons with a wave length of $\lambda = 546.1$ nm emitted by iron and neon ions of energy 1000 MeV/nucleon. The photons are generated in a quartz plate of

thickness $L = 5$ mm. Here a decrease in specific energy losses results in narrower angular distributions of radiation, but spectra keep their diffraction structure up to $Z = 10$.

The multiple scattering effects that we neglect may cause a partially or completely smoothed diffraction pattern predicted by formula (2). However, a more detailed analysis within the approach developed in ref. [3] shows that this negligence is justified to some extent when Cherenkov radiation from heavy ions of not very high energy (a few times hundred MeV per nucleon) is considered. The results of more complete investigations involving influence of both elastic and inelastic processes in the radiator will be published soon.

The authors are very grateful to Dr.V.P.Zrelov and Professors M.I.Podgoretsky and M.P.Rekalo for their interest in this work and for fruitful discussions.

References

1. Tamm I.E., Frank I.M. — Doklady AN SSSR, 1937, 14, p.107.
2. Dedrick K.G. — Phys. Rev., 1952, 87, p.891.
3. Kuzmin E.S., Tarasov A.V. — JINR Communication P1-92-525, Dubna, 1992.

Received on September 20, 1993.

УДК 519.61

THE GAUGED NONLINEAR SCHRÖDINGER EQUATION ON THE PLANE: A REGULARIZED MODEL WITH VORTEX SOLUTIONS

I.V.Barashenkov[1], A.O.Harin[2]

We consider a complex scalar field interacting with the Chern — Simons gauge field in 2+1 dimensions. In the relativistic case this model is known to support vortexlike solutions. However, its nonrelativistic counterpart was found not to possess even the condensate (i.e. spatially uniform) solution. Here we propose a new self-consistent nonrelativistic Chern — Simons gauge theory which does have both the condensate solution and a variety of vortex- and bubblelike solitons. When the scalar self-interaction is ϕ^4, the solutions satisfy self-duality equations.

The investigation has been carried out at the Laboratory of Computing Techniques and Automation, JINR, University of Cape Town and University of Natal (Durban).

Нелинейное уравнение Шредингера с калибровочным полем на плоскости: регуляризованная модель с вихревыми решениями

И.В.Барашенков, А.О.Харин

Рассматривается комплексное скалярное поле, взаимодействующее с калибровочным полем Черна — Саймонса в (2+1)-мерном пространстве. Известно, что, хотя в релятивистском случае эта модель допускает вихревые решения, ее нерелятивистский вариант не описывает даже конденсат, т.е. пространственно-однородное состояние. В настоящей заметке предлагается новая самосогласованная нерелятивистская модель с членом Черна — Саймонса, обладающая как конденсатным решением, так и набором топологических и нетопологических солитонов. В случае взаимодействия ϕ^4, решения удовлетворяют уравнениям самодуальности.

Работа выполнена в Лаборатории вычислительной техники и автоматизации ОИЯИ, Кейптаунском и Натальском университетах.

[1]Joint Institute for Nuclear Research and University of Cape Town; E-mail: igor@uctvax.uct.ac.za

[2]University of Natal, Durban; E-mail: harin@ph,und.ac.za

Introduction. Recently there has been much interest in (2+1)-dimensional gauge theories with the Chern-Simons term. The Chern-Simons theories were proposed in the context of condensed matter physics to describe low-energy phenomena in quasiplanar systems of anyons, particles with fractional statistics. These phenomena include e. g. the high-T_c superconductivity and the fractional quantum Hall effect.

The role of the anyonlike objects is played by vortices, topologically nontrivial two-dimensional localized structures. Accordingly vortex solutions have been in the focus of mathematical studies of the Chern-Simons theories. Most progress, so far, has been made in the relativistic case, when the matter field satisfies the nonlinear Klein-Gordon equation. As far as the nonrelativistic limit is concerned (which is of course more attractive for applications), only nontopological, "bell-like" solitons were found [1]. Furthermore, it can readily be shown [2] that even the *condensate* (i. e. nonzero constant solution) is not admitted by the nonrelativistic model introduced in [1].

In the present note we demonstrate that this drawback originates in the fact that the gauged nonlinear Schrödinger equation in its standard form [1] is not suitable for describing *dark solitons*, i.e. solitons with the nonvanishing background, such as vortices and bubbles. Accordingly, we propose a new version of the model which is completely compatible with the nonvanishing ("condensate") boundary conditions. As its predecessor, the new model is self-consistent: the conserved matter current serves as a source of the gauge field.

Inadequacy of the standard model. The failure of the standard nonrelativistic model [1] to possess even the condensate solution can be traced back to its Lagrangian formulation. This drawback is inherited from the nongauged version of the model.

Indeed, consider the one-dimensional nonlinear Schrödinger equation with a general nonlinearity,

$$i\phi_t + \phi_{xx} + F(\rho)\phi = 0. \tag{1}$$

Here $\rho = |\phi|^2$, and $F(\rho) = -dU/d\rho$. The standard Lagrangian for eq. (1),

$$\mathcal{L} = \frac{i}{2}(\phi_t\phi^* - \phi_t^*\phi) - |\phi_x|^2 - U(\rho), \tag{2}$$

does not *automatically* produce correct integrals of motion for solutions with nonvanishing boundary conditions. First of all, the number of particles integral,

$$N = \int \left(\frac{\partial \mathcal{L}}{\partial \phi_t} i\phi - \frac{\partial \mathcal{L}}{\partial \phi_t^*} i\phi^* \right) dx, \tag{3}$$

corresponding to the global $U(1)$ invariance of the system, takes the form $N = \int \rho \, dx$. This integral, of course, diverges for solutions with $|\phi|^2$ approaching ρ_0 at infinity. The regularized number of particles,

$$N = \int (\rho - \rho_0) \, dx, \tag{4}$$

is obtained by the *ad hoc* subtraction of the background contribution.

The standard definition of momentum,

$$P = \int \left(\phi_x \frac{\partial \mathcal{L}}{\partial \phi_t} + \phi_x^* \frac{\partial \mathcal{L}}{\partial \phi_t^*} \right) dx, \tag{5}$$

does not yield the correct expression either. For the Lagrangian (2) one obtains $P = \frac{i}{2} \int (\phi \phi_x^* - \phi^* \phi_x) \, dx$. It appears that this definition is not compatible with the Hamiltonian structure of the model [4]. Indeed, varying P gives

$$\delta P = i \int (\phi_x^* \delta\phi - \phi_x \delta\phi^*) dx + \rho_0 \delta \operatorname{Arg} \phi \Big|_{-\infty}^{+\infty}.$$

The appearance of the boundary term here makes it impossible to find the functional derivatives $\delta P / \delta \phi$ and $\delta P / \delta \phi^*$. Consequently, the Poisson bracket of P with some other functional, e. g. Hamiltonian, cannot be evaluated. The only definition compatible with the Hamiltonian structure of the model is*

$$P = \frac{i}{2} \int (\phi \phi_x^* - \phi^* \phi_x) \, dx - \rho_0 \operatorname{Arg} \phi \Big|_{-\infty}^{+\infty}$$

$$= \int (\phi_x^* \phi - \phi_x \phi^*) \left(1 - \frac{\rho_0}{\rho} \right) dx. \tag{6}$$

*It is appropriate to note that it was this modified definition of momentum that permitted the formulation of a stability criterion for moving dark solitons [3], [4].

Proceeding to two dimensions, the standard definition

$$P = \frac{i}{2}\int (\phi\nabla\phi^* - \phi^*\nabla\phi)\, d^2r \tag{7}$$

is even less suitable, since in general the integral (7) diverges.

Now the gauged nonlinear Schrödinger equation reads

$$i\phi_t - eA_0\phi + \mathbf{D}^2\phi + F(\rho)\phi = 0, \tag{8}$$

where $D_\mu = \partial_\mu + ieA_\mu$ and the Abelian gauge field A_μ satisfies

$$\kappa\partial_\beta F^{\beta\alpha} + \frac{\mu}{2}\epsilon^{\alpha\beta\gamma}F_{\beta\gamma} = eJ^\alpha. \tag{9}$$

Here $J^\mu = (J_0, \mathbf{J})$ designates the conserved matter current:

$$J_0 = \rho = |\phi|^2, \tag{10}$$

$$\mathbf{J} = \frac{1}{i}\{\phi^*(\mathbf{D}\phi) - \phi(\mathbf{D}\phi)^*\}, \tag{11}$$

$F_{\mu\nu} = \partial_\mu A_\nu - \partial_\nu A_\mu$, Greek and Latin indices run over 0,1,2 and 1,2, respectively. The parameter e is a gauge coupling, and κ and μ control the relative contributions of the Maxwell and Chern-Simons terms in the corresponding Lagrangian:

$$\mathcal{L} = \frac{i}{2}(\phi^*(D_0\phi) - \phi(D_0\phi)^*) - (D_k\phi)^*(D_k\phi) - \frac{\kappa}{4}F_{\mu\nu}F^{\mu\nu} + \frac{\mu}{4}\epsilon^{\mu\alpha\beta}A_\mu F_{\alpha\beta} - U(\rho). \tag{12}$$

This system inherits the drawback of its nongauged counterpart. The momentum, defined by

$$P_i = \int \left[\frac{\partial\phi}{\partial x^i}\frac{\partial\mathcal{L}}{\partial\phi_t} + \frac{\partial\phi^*}{\partial x^i}\frac{\partial\mathcal{L}}{\partial\phi_t^*} + \frac{\partial A^\alpha}{\partial x^i}\frac{\partial\mathcal{L}}{\partial A_t^\alpha}\right] d^2r, \tag{13}$$

equals

$$P_i = \int \left[\frac{i}{2}(\phi D_i\phi^* - \phi^* D_i\phi) - \kappa\epsilon_{ij}E^jB\right] d^2r = \int \rho\,(\partial_i \mathrm{Arg}\,\phi - eA^i)\, d^2r - \kappa\int \epsilon_{ij}E^jB\, d^2r. \tag{14}$$

Here $\mathbf{E} = -\nabla A_0$ is electric and $B = -F_{12}$ magnetic fields. The momentum in this case is finite, provided $A^i \to \frac{1}{e}\partial_i \mathrm{Arg}\,\phi$ at infinity. However, the functional derivatives $\delta P_i/\delta\phi$ and $\delta P_i/\delta\phi^*$ still cannot be calculated.

The new model. Thus, a natural question is: Is it possible to find a Lagrangian producing the same Euler-Lagrange equations as (2) but at the same time yielding the correct integrals of motion? We claim that the Lagrangian

$$\mathcal{L} = \frac{i}{2}(\phi_t\phi^* - \phi_t^*\phi)\left(1 - \frac{\rho_0}{\rho}\right) - |\phi_x|^2 - U(\rho), \tag{15}$$

satisfies both these requirements. It produces the same NLS (1), while formulas (3) and (5) yield the correct integrals N and P, as given exactly by (4) and (6).

We propose to adopt the Lagrangian (15) as the basis for the nonrelativistic gauge theory. In two dimensions, and after the introduction of the Chern-Simons – Maxwell gauge field, it takes the following form:

$$\mathcal{L} = \frac{i}{2}(\phi^*(D_0\phi) - \phi(D_0\phi)^*)\left(1 - \frac{\rho_0}{\rho}\right) - (D_k\phi)^*(D_k\phi) - \frac{\kappa}{4}F_{\mu\nu}F^{\mu\nu} + \frac{\mu}{4}\epsilon^{\mu\alpha\beta}A_\mu F_{\alpha\beta} - U(\rho). \tag{16}$$

As expected, this Lagrangian produces the correct number of particles,

$$N = \int(\rho - \rho_0)\,d^2r, \tag{17}$$

and momentum compatible with the Hamiltonian structure of the model:

$$P_i = \int\left[\frac{i}{2}(\phi D_i\phi^* - \phi^* D_i\phi)\left(1 - \frac{\rho_0}{\rho}\right) - \kappa\epsilon_{ij}E^jB\right]d^2r = \int(\rho - \rho_0)\left[\partial_i \mathrm{Arg}\,\phi - eA^i\right]d^2r + \kappa\int\epsilon_{ij}E^jB\,d^2r. \tag{18}$$

The field equations resulting from (16) however differ from those of the standard model (12). The difference lies in the definition of the density of the number of particles [the charge component of the vector $J^\mu = (J_0, \mathbf{J})$]:

$$J_0 = \rho - \rho_0. \tag{19}$$

Other than that, the field equations are the same, eqs. (8), (9), with the spatial part of the current being given by the standard expression (11). The Hamiltonian of the modified system has the standard

form:

$$H = \int \left[|\mathbf{D}\phi|^2 + U(\rho) + \frac{\kappa}{2}(\mathbf{E}^2 + B^2) \right] d^2r. \qquad (20)$$

The difference in the definition of J_0, however, drastically changes the properties of the model. It turns out that the modified model not only possesses the condensate solution but also exhibits a self-dual limit and a rich variety of vortex and bubble-like solitons.

Acknowledgments. This work was supported by the Foundation for Research Development of South Africa and a research grant from the University of Cape Town. It is a pleasure to thank Professor Peter Leach and Professor Igor Puzynin for their continual support and encouragement.

REFERENCES

[1] R. Jackiw and S.-Y. Pi, Phys. Rev. Lett. **64**, 2969 (1990); Phys. Rev. D **42**, 3500 (1990).

[2] I. V. Barashenkov and A. O. Harin, No-go theorems for gauged solitonic bubbles, Preprint 1993/4, Institute of Theoretical Physics and Astrophysics, UCT, Cape Town, 1993.

[3] M. M. Bogdan, A. S. Kovalev, and A. M. Kosevich, Fiz. Nizk. Temp. **15**, 511 (1989).

[4] I. V. Barashenkov and E. Yu. Panova, Physica D, in press.

Received on September 14, 1993.